



1 **Low levels of nitryl chloride: Nocturnal nitrogen oxides in**
2 **the Lower Fraser Valley of British Columbia**

3 **Hans D. Osthoff¹, Charles A. Odame-Ankrah¹, Youssef M. Taha¹,**
4 **Travis W. Tokarek¹, Corinne L. Schiller², Donna Haga³, Keith Jones², and**
5 **Roxanne Vingarzan²**

6 [1] {Department of Chemistry, University of Calgary, Calgary, Alberta T2N 1N4,
7 Canada}

8 [2] {Applied Science Division, Prediction and Services West, Meteorological Service of
9 Canada, Environment and Climate Change Canada, Vancouver, British Columbia V6C
10 3S5, Canada}

11 [3] {British Columbia Ministry of Environment and Climate Change Strategy,
12 Cranbrook, British Columbia V1C 7G5, Canada}

13 Correspondence to: H. D. Osthoff (hosthoff@ucalgary.ca)

14 **Abstract**

15

16 The nocturnal nitrogen oxides, which include the nitrate radical (NO₃), dinitrogen pentoxide
17 (N₂O₅), and its uptake product on chloride containing aerosol, nitryl chloride (ClNO₂), can have
18 profound impacts on the lifetime of NO_x (= NO + NO₂), radical budgets, and next-day
19 photochemical ozone (O₃) production, yet their abundances and chemistry are only sparsely
20 constrained by ambient air measurements.

21 Here, we present a measurement data set collected at a routine monitoring site near the
22 Abbotsford International Airport (YXX) located approximately 30 km from the Pacific Ocean
23 in the Lower Fraser Valley (LFV) on the West coast of British Columbia. Measurements were
24 made from July 20 to August 4, 2012, and included mixing ratios of ClNO₂, N₂O₅, NO, NO₂,
25 total odd nitrogen (NO_y), O₃, photolysis frequencies, and size distribution and composition of
26 non-refractory submicron aerosol.

27 At night, O₃ was rapidly and often completely removed by dry deposition and by titration with
28 NO of anthropogenic origin and unsaturated biogenic hydrocarbons in a shallow nocturnal



29 inversion surface layer. The low nocturnal O₃ mixing ratios and presence of strong chemical
30 sinks for NO₃ limited the extent of nocturnal nitrogen oxide chemistry at ground level.
31 Consequently, mixing ratios of N₂O₅ and ClNO₂ were low (<30 and <100 parts-per-trillion by
32 volume (pptv) and median nocturnal peak values of 7.8 pptv and 7.9 pptv, respectively). Mixing
33 ratios of ClNO₂ frequently peaked 1 - 2 hours after sunrise rationalized by more efficient
34 formation of ClNO₂ in the nocturnal residual layer aloft than at the surface and the breakup of
35 the nocturnal boundary layer structure in the morning. When quantifiable, production of ClNO₂
36 from N₂O₅ was efficient and likely occurred predominantly on unquantified supermicron sized
37 or refractory sea salt derived aerosol. After sunrise, production of Cl radicals from photolysis
38 of ClNO₂ was negligible compared to production of OH from the reaction of O(¹D) + H₂O
39 except for a short period after sunrise.

40

41 **Keywords**

42 Lower Fraser Valley, ClNO₂, surface measurements, nocturnal residual layer, ClNO₂ morning
43 peak, vertical entrainment

44



45 1 Introduction

46 The Lower Fraser Valley (LFV) is prone to episodes of poor air quality, in part because of its
47 geography which facilitates stagnation periods and accumulation of airborne pollutants through
48 processes such as the Wake-Induced Stagnation Effect (Brook et al., 2004), and also because
49 of continued growth of human population and associated emissions from urban, suburban,
50 agricultural and marine sources. Of special concern have been repeated exceedances of the
51 Canada-Wide Standard and, as of 2012, the Canadian Ambient Air Quality Standards (CAAQS)
52 for fine particulate matter (PM_{2.5}) and ozone (O₃) at Chilliwack and Hope, located in the eastern
53 part of the LFV downwind of Vancouver (Ainslie et al., 2013). These exceedances have
54 occurred in spite of ongoing declines in emissions of both nitrogen oxides (NO_x = NO + NO₂)
55 and volatile organic compounds (VOCs) resulting from the introduction of new vehicle
56 standards and (now discontinued) local vehicle emission testing programs (Ainslie et al., 2013).
57 Previous large-scale studies in the LFV such as Pacific 1993 (Steyn et al., 1997), the Regional
58 Visibility Experimental Assessment in the Lower Fraser Valley (REVEAL) I and II (Pryor et
59 al., 1997; Pryor and Barthelmie, 2000) and Pacific 2001 (Vingarzan and Li, 2006) have added
60 important information regarding atmospheric processes leading to O₃ and aerosol formation
61 and visibility issues. However, the transformation of primary (e.g., NO_x, VOCs, SO₂, NH₃, etc.)
62 to secondary pollutants (i.e., O₃ and fine particulate matter) is highly complex, and the
63 scientific understanding of these highly non-linear processes remains incomplete.

64 A complicating factor in the LFV is the interaction of anthropogenic emissions with marine
65 derived sea salt aerosol. While sea spray aerosol is a primary source of particle matter (PM)
66 and hence directly affects particle concentration and mass loadings (Pryor et al., 2008), there is
67 now considerable evidence from modeling (Knipping and Dabdub, 2003), laboratory (Raff et
68 al., 2009), and field studies (Tanaka et al., 2003; Osthoff et al., 2008) that "active chlorine"
69 species released from sea salt can negatively affect air quality and promote O₃ and secondary
70 aerosol formation in coastal regions.

71 In an analysis of 20 years of O₃ air quality data in the LFV region, *Ainslie and Steyn* (2007)
72 concluded that precursor buildup, prior to an exceedance day, plays an important role in the
73 spatial O₃ pattern on exceedance days. Secondary processes involving active chlorine produced
74 from the interaction of marine aerosol with anthropogenic pollution would fit this profile but
75 are not currently constrained by measurements.



76 One pathway to activate chlorine from sea salt is the reactive uptake of dinitrogen pentoxide
77 (N_2O_5) on chloride containing aerosol to yield nitryl chloride (ClNO_2). N_2O_5 is formed from
78 the reversible reaction of nitrogen dioxide (NO_2) with the photo-labile nitrate radical (NO_3),
79 which in turn is formed from reaction of NO_2 with O_3 .



82 During daytime, NO_3 (and, indirectly, N_2O_5) is removed primarily via its reaction with NO
83 (which is generated from NO_2 photolysis and directly emitted, for example, by automobiles)
84 and by NO_3 photolysis (Wayne et al., 1991).



87 The heterogeneous hydrolysis of N_2O_5 to nitric acid (HNO_3) is an important nocturnal NO_x and
88 odd oxygen ($\text{O}_x = \text{NO}_2 + \text{O}_3$) removal pathway (Chang et al., 2011; Brown et al., 2006a). On
89 chloride containing aerosol, however, uptake of N_2O_5 yields up to a stoichiometric amount of
90 ClNO_2 (Behnke et al., 1997; Finlayson-Pitts et al., 1989):



92 The ClNO_2 yield, ϕ , is primarily a function of aerosol chloride and water content (Behnke et
93 al., 1997; Bertram and Thornton, 2009; Roberts et al., 2009; Ryder et al., 2014; Ryder et al.,
94 2015b; Ryder et al., 2015a). Formation of ClNO_2 impacts air quality in the following ways:
95 Since ClNO_2 is long-lived at night (Osthoff et al., 2008), its primary fate is photo-dissociation
96 (to Cl and NO_2) in the morning hours after sunrise.



98 This reaction increases the morning abundance of O_x , leading to greater net photochemical O_3
99 production throughout the day. The other photo fragment, the Cl atom, is highly reactive
100 towards hydrocarbons and will initiate radical chain reactions that produce O_3 and secondary
101 aerosol (Behnke et al., 1997; Young et al., 2014). The fate and impact of ClNO_2 is thus similar
102 to that of nitrous acid (HONO), which also accumulates during the night and photodissociates
103 in the morning to release NO and the hydroxyl radical (OH) that go on to produce O_3 (Alicke
104 et al., 2003).



105 Data collected during the 2006 Texas Air Quality Study – Gulf of Mexico Atmospheric
106 Composition and Climate Study (TEXAQS-GOMACCS) have shown that ClNO₂ production
107 is efficient in the nocturnal polluted marine boundary layer even on primarily non-sea salt
108 aerosol surfaces. As a result, up to 15% of total odd nitrogen (NO_y) was present in the form
109 ClNO₂ at night (Osthoff et al., 2008). The high efficiency of ClNO₂ formation on aerosol of
110 medium-to-low total chloride content has been confirmed by several laboratory investigations
111 (Bertram and Thornton, 2009; Raff et al., 2009; Roberts et al., 2009) and direct measurements
112 of N₂O₅ uptake on ambient particles (Riedel et al., 2012b). Some ambiguity remains as to the
113 detailed mechanism of the reaction, but there is agreement that acid displacement of HCl from
114 supermicron (predominantly sea salt aerosol) to submicron (predominantly non-sea salt
115 aerosol) is a key step in the efficient production of ClNO₂. These results suggested that this
116 chemistry is active anywhere where pollution in the form of NO_x and O₃ comes in contact with
117 marine air, including the LFV.

118 However, while the yield of ClNO₂ in reaction (5) is high in polluted coastal regions, the ClNO₂
119 yield relative to the amount of NO₃ produced from reaction (1) cannot be easily predicted
120 because NO₃ is consumed by reactions with VOCs, e.g., biogenic VOCs such as isoprene and
121 monoterpenes as well as aldehydes, and dimethyl sulfide (Wayne et al., 1991).



123 Previous studies in the LFV have shown high biogenic VOC concentrations (Biesenthal et al.,
124 1997; Gurren et al., 1998; Drewitt et al., 1998) yet there was active nighttime nitrogen oxide
125 chemistry. During the Pacific 2001 study, measurements of the mixing ratios of NO, NO₂,
126 peroxyacetic nitric anhydride (CH₃C(O)O₂NO₂, PAN), HONO, HNO₃, and NO_y at three ground
127 sites in the LFV indicated deficits of up to 15% in the nocturnal NO_y budget (Hayden et al.,
128 2004) attributable to unquantified species such as alkyl nitrates, N₂O₅, and ClNO₂. McLaren
129 and coworkers quantified mixing ratios of NO₂ and NO₃ by differential optical absorption
130 spectroscopy (DOAS) at the Sumas Eagle Ridge site (~250 m above the floor of the LFV) as
131 part of Pacific 2001 (McLaren et al., 2004) and off-shore on Saturna Island (Figure 1) in the
132 Strait of Georgia in 2005 (McLaren et al., 2010). The LFV data showed occasional episodes of
133 active nocturnal nitrogen oxide chemistry in the residual layer with N₂O₅ contributing up to 9%
134 of NO_y, while the Saturna Island data showed NO₃ mixing ratios of > 20 parts-per-trillion by
135 volume (10⁻¹², pptv) every night of measurement. McLaren *et al.* estimated that between 0.3
136 and 1.9 ppbv of ClNO₂ would be produced under these conditions (McLaren et al., 2010).



137 Efficient formation of ClNO₂ would be consistent with the unidentified O₃ precursor proposed
138 by *Ainslie and Steyn* and is also a plausible explanation for part of the deficit in the NO_y budget
139 observed by *Hayden et al.* (2004).

140 Another feature of the LFV are somewhat unusual diurnal profiles arising from the vertical
141 structure in pollutant concentrations. Measurements of O₃ and NO₂ using tethered balloons by
142 *Pisano et al.* (1997) during Pacific 93 at the Harris Road site (located ~38 km NW of Abbotsford
143 International Airport) revealed a highly stratified boundary layer with a shallow, 50 m deep
144 isothermal surface layer (also called a nocturnal boundary layer, or NBL) and low surface O₃
145 concentrations at night. Nocturnal loss of surface O₃ is known to occur by several pathways,
146 including dry deposition, titration with NO, and reaction with unsaturated biogenic
147 hydrocarbons (*Neu et al.*, 1994; *Kleinman et al.*, 1994; *Trainer et al.*, 1987; *Logan*, 1989; *Talbot*
148 *et al.*, 2005). Titration of O₃ with NO is readily quantified as the concentration of a product of
149 this reaction, NO₂, can be measured directly and conserves O_x.



151 Usually, the major nocturnal sink of O_x is dry deposition of O₃ and NO₂ (*Lin et al.*, 2010).

152 The balloon data also showed pools of NO₂ and O₃ in a ~100 m deep nocturnal residual layer
153 (NRL) located 200 to 350 m above ground. Following the break-up of the nocturnal layers in
154 the early morning, vertical down-mixing events of O₃ pollution were observed (*McKendry et*
155 *al.*, 1997). In this process, pollutants are entrained into the growing mixed layer from the NRL,
156 i.e., the growing mixed layer in the hours after sunrise erodes the somewhat deeper NRL, and
157 pollutants are mixed to the surface (*Neu et al.*, 1994; *Kleinman et al.*, 1994).

158 In this manuscript, we present the first measurements of ClNO₂ and N₂O₅ mixing ratios in the
159 LFV. The data were collected at a surface site east of the Abbotsford International Airport
160 (International Air Transport Association (IATA) airport code YXX) located approximately
161 35 km from the Pacific Ocean from July 20 to August 5, 2012. Auxiliary measurements
162 included NO, NO₂, NO_y, O₃, photolysis frequencies, and submicron aerosol composition and
163 size distributions. An analysis of nocturnal nitrogen oxide chemistry including the formation of
164 ClNO₂ and its potential impact on nocturnal O₃ and NO₂ loss and radical budgets in the LFV
165 are presented.

166

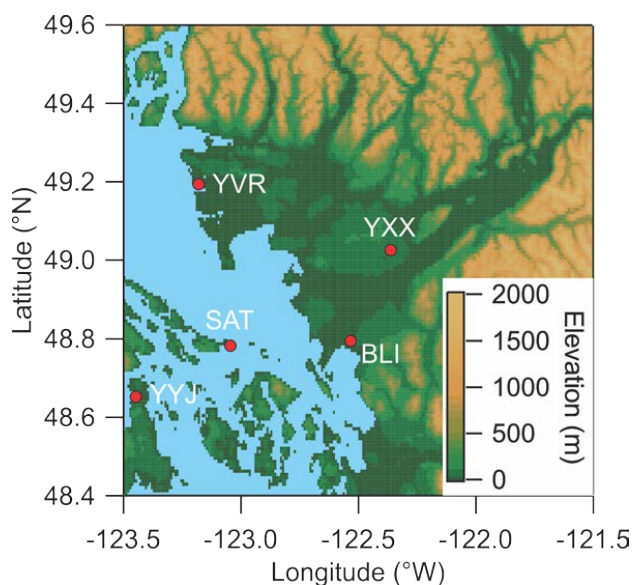


167 2 Experimental

168 2.1 Location

169 The map shown in Figure 1 indicates the location of the study. Ambient air measurements were
170 conducted at the T45 routine monitoring site located to the east YXX at latitude 49.0212 (N)
171 and longitude -122.3267 (W) and ~60 m above sea level (ASL) and ~30 km from the Pacific
172 Ocean. A raspberry field was located immediately to the W between the end of the airport
173 runway and the measurement site. Nearby local sources included agricultural operations (such
174 as poultry farms) and emissions from motor vehicle traffic on secondary roads and highways.
175 YXX is located ~60 km ESE of the Vancouver International Airport (YVR) and the City of
176 Vancouver. Abbotsford is in the heart of the so-called "Lower Mainland", the low-lying region
177 stretching from Pacific Ocean at Vancouver to the NW and the Canada-USA border to the S
178 (north of Bellingham, BLI) to the eastern end of the Fraser Valley with a total population in
179 excess of 2,500,000.

180



181

182 **Figure 1.** Map of the Lower Fraser Valley. YXX = Abbotsford International Airport
183 (measurement location for this study). YVR = Vancouver Int'l Airport. YYJ = Victoria Int'l
184 Airport. BLI = Bellingham Int'l Airport. SAT = Saturna Island.

185



186 2.2 Measurement techniques

187 The measurement techniques used for this study are listed in Table 1. Data were averaged to 5
188 min prior to presentation.

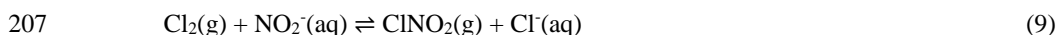
189 The instruments measuring O₃ and nitrogen oxides were housed in an air-conditioned trailer
190 and sampled from a common 0.635 cm (¼") outer diameter (o.d.) and 0.476 cm (3/16") inner
191 diameter (i.d.) Teflon™ inlet at a height of 4 m above ground; the setup is depicted in Figure 3
192 of Tokarek *et al.* (2014). A scroll pump whose flow rate was throttled using a 50 standard liters
193 per minute (slpm) capacity mass flow controller was connected to the end of the common inlet
194 to minimize the residence time of the sampled air and to reduce inlet "ageing", i.e.,
195 accumulation of aerosol on filters of individual instruments, whose inlets tapped into the main
196 inlet line at 90°. The total inlet flow was in the range of 18 to 20 slpm.

197 Measurements of aerosol composition and size distributions and of meteorological data were
198 made from the research trailer housing the routine measurements at the site. The Agilent VOC
199 measurements were made from a research trailer owned by ECCC.

200

201 2.2.1 Quantification of ClNO₂ by iodide chemical ionization mass spectrometry

202 Mixing ratios of ClNO₂ were quantified as iodide cluster ions at *m/z* 208 using the THS iodide
203 chemical ionization mass spectrometer (iCIMS) described by Mielke *et al.* (2011) and calibrated
204 using the scheme by Thaler *et al.* (2011). In this method, a gas stream containing ClNO₂ is
205 generated from reaction of Cl₂ (Praxair, 10 ppmv in N₂) with an aqueous slurry saturated with
206 NaNO₂ (Sigma-Aldrich):



208 This gas stream was periodically added to the main inlet with the aid of a normally-open 2-way
209 valve connected to a vacuum pump in a similar fashion as described earlier for N₂O₅ and PAN
210 (Tokarek *et al.*, 2014; Odame-Ankrah and Osthoff, 2011). The ClNO₂ content of the calibration
211 gas stream was quantified by thermal dissociation cavity ring-down spectroscopy (TD-CRDS)
212 as described in section 2.2.2. In total, 31 calibrations for ClNO₂ were carried out, spread out
213 evenly over the measurement period. The iCIMS response factor at *m/z* 208 was (0.40±0.06)
214 Hz pptv⁻¹ (where the error represents the standard deviation of repeated calibrations),
215 normalized to 10⁶ counts of reagent ion at *m/z* 127. The ³⁷ClNO₂I⁻ ion at *m/z* 210 was also
216 monitored and found to be (0.298±0.004) times the signal at *m/z* 208 (*r*² = 0.944), slightly lower



217 than Standard Mean Ocean Chloride ^{37}Cl mole fraction in sea water of ~ 0.319 (Wieser and
218 Berglund, 2009) and our previously observed ratios of 0.315 ± 0.003 in Calgary (Mielke et al.,
219 2011) and 0.3065 ± 0.0002 in Pasadena (Mielke et al., 2013). The reason(s) for these differences
220 are unclear but may be a result of fractionation processes (Koehler and Wassenaar, 2010; Volpe
221 et al., 1998), a topic outside the scope of this manuscript.

222 The iCIMS was also used to quantify mixing ratios of PAN at m/z 59 and PPN at m/z 73 (Slusher
223 et al., 2004; Mielke et al., 2011; Mielke and Osthoff, 2012). For this reason, part of the
224 instrument's inlet prior to the ion-molecule reaction region was heated to $190\text{ }^\circ\text{C}$ to dissociate
225 PANs into their respective carboxylates. Further, the collisional dissociation chamber (CDC)
226 was operated in declustering mode (-22.7 V) to break up ion clusters. Calibrations and matrix
227 effect correction procedures and a time series of the PAN and PPN data were presented by
228 Tokarek et al. (2014).

229

230 2.2.2 Quantification of NO_2 and N_2O_5 by cavity ring-down spectroscopy

231 The CRDS used in this work was an amalgamated version of two instruments described earlier
232 (Paul and Osthoff, 2010; Odame-Ankrah and Osthoff, 2011), called "Improved Detection
233 Instrument for Nitrogen Oxide Species" (iDinos) (Odame-Ankrah, 2015). A schematic of the
234 optical layout is shown in Figure 2. The optical bread board, instrument frame, electronic and
235 data acquisition components were as described by Paul and Osthoff (2010). The new instrument
236 was set up with up to six parallel detection channels: four 405 nm "blue" diode laser CRDS
237 cells for quantification at NO_2 via its absorption at 405 nm with a distance between the pairs of
238 high-reflectivity (HR) mirrors (Advanced Thin Films) of 112.5 cm , of which 92.0 cm were
239 filled with sample air, and two newly constructed 662 nm "red" diode laser CRDS cells for
240 quantification at NO_3 via its absorption at 662 nm with a distance between the HR mirrors (Los
241 Gatos) of 93.0 cm of which 73.0 cm were filled with sample air. Light exiting the far ends of
242 the CRDS cells was collected using fixed-focus collimating lenses and multimode optical fibers
243 (Thorlabs) connected to photomultiplier tubes (PMT, Hamamatsu H9433-03MOD) with 10
244 MHz bandwidth. Bandpass filters (Thorlabs FB405-10 and FB660-10) were placed between
245 the PMTs and the end of the optical fibers.

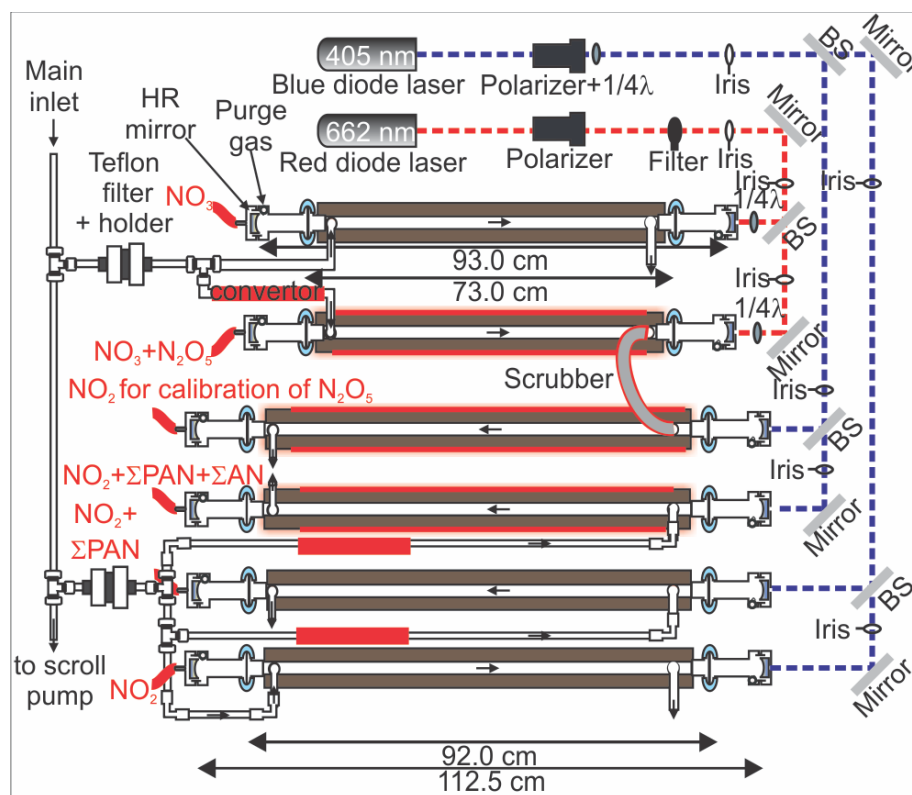
246 The two laser diodes were simultaneously square-wave modulated by a function generator (SRS
247 DS335). The PMT voltages were digitized using an 8-channel 14-bit data acquisition card
248 (National Instruments PCI-6133; 2.5 MS s^{-1} simultaneous sampling sample rate) connected to



249 a laptop computer via a PCMCIA-to-PCI expansion unit (Magma CB4DRQ) and controlled by
 250 software written in LABVIEW™ (National Instruments).

251 Ring-down time constants (τ) were determined from a linear fit to the logarithm of the digitized
 252 PMT voltage as described by *Brown et al.* (2002) immediately after acquisition of the ring-
 253 down traces (which were co-added to a user-selectable averaging time prior to the fit). The
 254 fitting algorithm requires the subtraction of the PMT voltage offset prior to taking the logarithm;
 255 this offset was measured between ring-down events after the signal had returned to baseline,
 256 which limited the repetition rate of the diode lasers and the number of traces averaged per
 257 second to a frequency of 300 Hz.

258



259

260 **Figure 2.** Optical layout of the cavity ring-down spectrometer. $\frac{1}{4}\lambda$ = quarter wave plate. BS =
 261 beam splitter. HR mirror = high reflectivity mirror. Drawing is not to scale.

262



263 Ring-down time constants in the absence of the target absorber (τ_0) were determined by
264 flooding the inlet (each once per hour) with ultra-pure, or "zero", air (Praxair) for the 405 nm
265 channels and by titration with NO for the 662 nm channel (Brown et al., 2001; Simpson, 2003)
266 Typical values of τ_0 were in the range of 63 to 67 μs and between 198 and 210 μs for the blue
267 and red channels, respectively. The baseline precision (i.e., standard deviation, σ) of the NO₂
268 and NO₃ measurements were ± 80 pptv and ± 3 pptv (1 s data), respectively. For the NO₃
269 channels, additional noise was introduced by variable background absorption of NO₂, O₃, and
270 water vapor which produce small, spurious structure in the 662 nm absorption signal (Dubé et
271 al., 2006) and were not tracked well by the interpolation of the baseline from the hourly τ_0
272 determinations.

273 During the Abbotsford campaign, only five (four blue and one red) CRDS channels were
274 operated because of delays in the fabrication of the final set of CRDS mirror holders. The
275 662 nm CRDS cell sampled from a Teflon™ inlet heated to 130 °C for quantification of NO₃
276 plus the NO₃ generated from thermal dissociation N₂O₅ (Brown et al., 2001; Simpson, 2003;
277 Dubé et al., 2006). Under the high-NO_x conditions of this study, equilibrium (2) was sufficiently
278 far to the right (see section 3.3) such that $[\text{NO}_3] + [\text{N}_2\text{O}_5] \approx [\text{N}_2\text{O}_5]$, i.e., the concentration
279 measured could be equated with $[\text{N}_2\text{O}_5]$ without introducing a large error (i.e., <5%). The four
280 405 nm CRDS cells were operated as follows: The first sampled from an ambient temperature
281 inlet and was used to quantify NO₂. The second sampled from a quartz inlet heated to 250 °C
282 and was used to quantify NO₂ plus total peroxyacyl nitrate (ΣPAN) (Paul et al., 2009; Paul and
283 Osthoff, 2010). Data from this channel will be presented in a future manuscript. The third was
284 operated with a quartz inlet heated to 450 °C to enable ClNO₂ calibrations (Thaler et al., 2011).
285 Quantification of total alkyl nitrates (ΣAN) in ambient air was not attempted because of the
286 high NO_x levels and resulting large subtraction errors (Thieser et al., 2016). The fourth 405 nm
287 CRDS cell was connected with polycarbonate tubing ($\frac{3}{8}$ " o.d. and $\frac{1}{4}$ " i.d.) in series to the
288 662 nm channel and was used to calibrate the response of the N₂O₅ channel, which is a function
289 of the transmission efficiency of N₂O₅ through the inlet and the overlap of the diode laser
290 spectrum with the NO₃ absorption line (Odame-Ankrah and Osthoff, 2011). The role of the
291 polycarbonate tube was to scrub NO₃ exiting the N₂O₅ channel, allowing detection of only the
292 NO₂ generated from thermal dissociation of N₂O₅ and to prevent recombination of NO₃ and
293 NO₂ in the blue calibration channel (Wagner et al., 2011).



294 N₂O₅ was generated in situ by adding an excess of O₃ (generated by passing O₂ past a 254 nm
295 Hg lamp) to nitric oxide (NO) in a 0.635 cm (¼") o.d. and 0.476 cm (3/16") i.d. Teflon™
296 calibration line and allowed to equilibrate (i.e., until the output was constant) offline before
297 being switched inline on demand. The N₂O₅ response varied between 65% and 100% depending
298 on inlet "age"; the Teflon™ inlet and aerosol inlet filter were changed every 2 – 3 days. The
299 accuracy of the NO₂ and N₂O₅ data were ±10% and ±25%, respectively, driven mainly by the
300 systematic uncertainty of the NO₂ absorption cross-section and of the N₂O₅ inlet transmission
301 efficiency (Odame-Ankrah, 2015).

302

303 2.2.3 Measurements of O₃, NO and NO_y,

304 Mixing ratios of O₃ were monitored by UV absorption in a commercial instrument (Thermo 49)
305 and were accurate within ±2% and ±1 ppbv. An NO-O₃ chemiluminescence instrument
306 (Thermo 42i) was used to monitor mixing ratios of NO and NO_y, which was reduced to NO in
307 a Mo converter heated to ~320 °C. This instrument sampled from the main inlet via a Teflon™
308 filter and filter holder and was calibrated daily against CRDS as described by *Tokarek et al.*
309 (2014). The slope uncertainty for each multipoint calibration was ±15%. Interpolation between
310 calibration runs gave an overall uncertainty of ±30%. The NO zero offset uncertainty (needed
311 for calculating the NO₃ loss rate with respect to reaction with NO) was ±10 pptv.

312

313 2.2.4 VOC measurements

314 Volatile organic compounds were monitored with a commercial gas chromatograph - mass
315 spectrometer (GC-MS; Agilent model 7890A and 5975C) equipped with an FID detector and a
316 Markes Unity 2 pre-concentrator with an ozone precursor trap cooled to -25 °C.

317 In a typical sampling sequence, a 500 mL air sample was collected at a flow rate of 25 mL
318 min⁻¹, taken from the center flow of a 1.27 cm (½") stainless steel inlet line which was
319 continuously sampling ambient air at 5 L min⁻¹. The sampled air flowed through a 0.318 cm
320 (1/8") stainless steel line and particles were removed using a 1 µm pore size fritted filter. Once
321 500 mL of air were collected, the pre-concentrator was flushed with helium to remove air while
322 awaiting injection. At the start of a GC run, the sample in the pre-concentrator was flash heated
323 to 300 °C and held for 3 min. The sample was separated on 2 columns with the entire sample



324 going through the Agilent VRX column with a Dean switch directing the first gases emitted to
325 a second GasPro column and then to the FID detector ($\sim < C_4$) while the heavier compounds
326 were detected using the MS detector in scan mode.

327 The cycle time for the GC analysis was 1 hour with the sample being collected during the
328 previous runs analyses. The 20 min sample was taken at the start of a 1 hour time period.

329 Due to the low temperature of the trap, the air was dried using a trap at $-30\text{ }^\circ\text{C}$. The trap was
330 heated and dried between each sample and reconditioned for 10 min prior to sample collection.
331 All sample lines were stainless steel with a Restek SulfinertTM coating to minimize sample loss
332 on the lines. Calibrations were performed once per day for 105 species using a 100 ppbv U.S.
333 Environmental Protection Agency (EPA) photochemical assessment monitoring system
334 (PAMS) and a 100 ppb EPA air method, toxic organics – 15 (TO15) standard tanks (Linde
335 Specialty Gases) at an approximately concentration of 2 ppbv. The terpenes were semi-
336 quantitatively measured as a calibration source was not available at the time and only the
337 changes in concentration strength with time of day used. The accuracy of the measurements
338 varied depending on the species but was better than $\pm 30\%$ throughout. Peaks were manually
339 reintegrated using Chemstation software from Agilent. Table S-1 summarizes the VOCs
340 quantified.

341

342 **2.3 Aerosol measurements**

343 The chemical composition of non-refractory submicron particulate matter was monitored using
344 an Aerosol Chemical Speciation Monitor (ACSM, Aerodyne), which reported concentrations
345 of NO_3^- , SO_4^{2-} , Cl^- , NH_4^+ , and total organics. A general description of this instrument designed
346 for routine monitoring has been given by Ng et al. (2011).

347 Submicron aerosol size distributions were quantified by a scanning mobility particle sizer
348 (SMPS, TSI 3034). This instrument measured aerosol particles in the range from 10 to 487 nm
349 using 54 size channels (32 channels per decade). Both of these instruments were housed in a
350 trailer operated by Metro Vancouver. The ACSM and the SMPS sampled air off a shared
351 stainless steel inlet that had a total flow of 5 L min^{-1} and contained a $\text{PM}_{2.5}$ sharpcut filter at the
352 inlet and was operated at ambient relative humidity.

353



354 **2.4 Photolysis frequencies**

355 Photolysis frequencies were determined by solar actinic flux spectroradiometry (Hofzumahaus
356 et al., 1999) using a commercial radiometer with 2π receptor optics and photo diode array
357 (PDA) detector (Metcon; 512 pixels, wavelength range 285 nm - 690 nm) calibrated by the
358 manufacturer. The spectrometer was mounted facing up (zenith view) and hence measured the
359 down-dwelling radiation. On several days, the spectrometer was inverted hourly to determine
360 the up-dwelling radiation, which was added to the down-dwelling flux. Photolysis frequencies
361 including $j(\text{NO}_3)$, $j(\text{NO}_2)$, $j(\text{O}^1\text{D})$, and $j(\text{ClONO}_2)$ were calculated using reference spectra and
362 quantum yields from (Sander et al., 2010) and (Ghosh et al., 2012). Table 2 gives the ratio of
363 observed up-dwelling to down-dwelling for selected photolysis frequencies. For August 3 (a
364 cloud-free day), the measurements were compared to (hourly) predictions with the online
365 "Tropospheric Ultraviolet and Visible (TUV) Radiation Model" V5.0 (Madronich and Flocke,
366 1997); with default settings, the model reproduced the measured $j(\text{NO}_2)$ and $j(\text{O}^1\text{D})$ quite well:
367 a scatter plot of observed against TUV rate constants had correlation coefficients (r) of 0.997
368 and 0.998, slopes of 1.06 ± 0.02 and 1.10 ± 0.02 , and offsets of $(3\pm 1)\times 10^{-4} \text{ s}^{-1}$ and $(5\pm 3)\times 10^{-7} \text{ s}^{-1}$.

369 **2.5 Box model simulations of the nocturnal O₃ and O_x loss in the NBL**

370 A box model was set up to reconcile the median nocturnal decays of O₃ and O_x. These
371 simulations are intended as back-of-the-envelope type estimates of major processes only since
372 an accurate description of the nocturnal boundary layer chemistry would require modeling of
373 horizontal and vertical transport, i.e., altitude-resolved information not available in this study
374 (Geyer and Stutz, 2004). The model's assumptions are a well-mixed NBL that is decoupled
375 from the NRL above it as observed by earlier balloon vertical profiling (Pisano et al., 1997), O₃
376 and NO₂ dry deposition velocities of $v_d(\text{O}_3) = 0.2 \text{ cm s}^{-1}$ and $v_d(\text{NO}_2) = \alpha v_d(\text{O}_3)$ with $\alpha=0.65$
377 (Lin et al., 2010), and negligible chemical O₃ and O_x losses other than titration of O₃ by NO
378 (reaction 8) and by reaction with a generic biogenic hydrocarbon (assumed to react with O₃
379 with a rate coefficient of $5\times 10^{-11} \text{ cm}^3 \text{ molec.}^{-1} \text{ s}^{-1}$, i.e., the rate coefficient for reaction of α -
380 pinene with O₃ (Seinfeld and Pandis, 2006)). Simulations were initiated with the median NO₂
381 and O₃ concentrations observed at sunset.

382



383 3 Results

384 3.1 Overview of data set

385 3.1.1 Meteorology

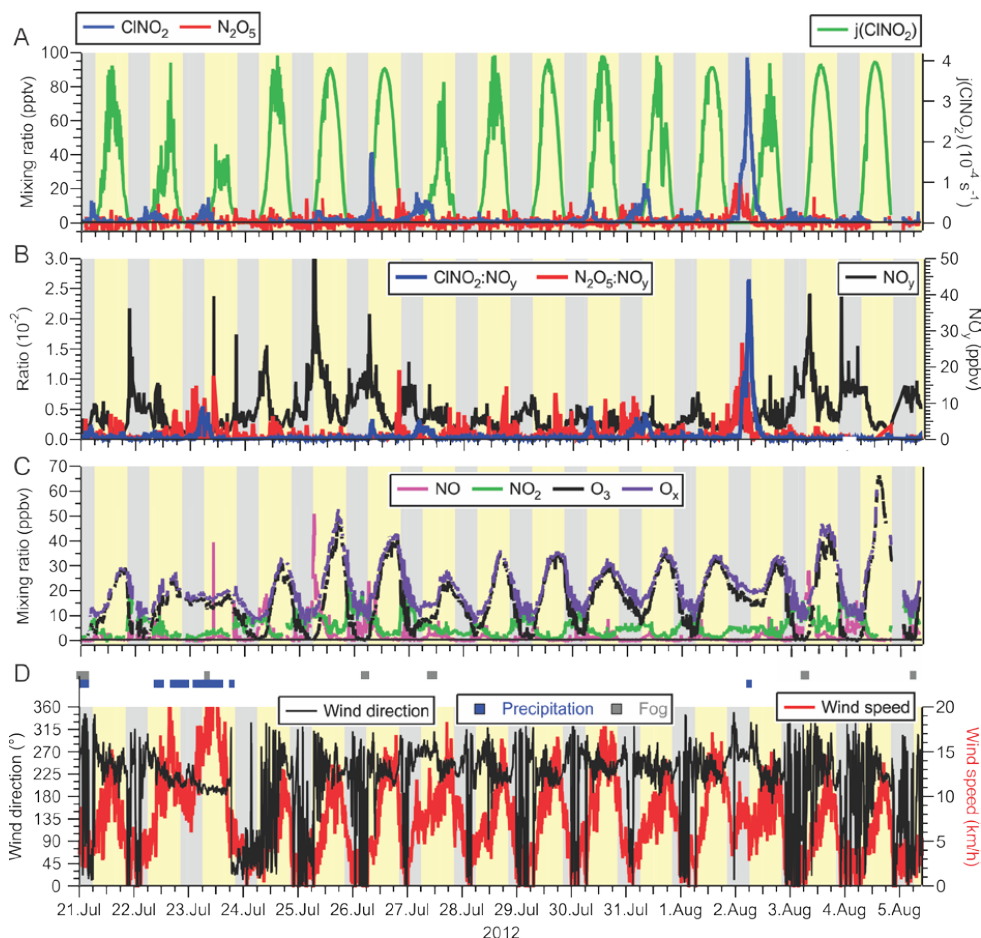
386 A time series of local wind direction and speed are displayed in Figure 3D. During the two-
387 week long measurement period, the air flow to the site was from the Pacific Ocean to the SW
388 and WSW with a moderate wind speed of 8.7 km hr^{-1} (median value). On most nights, local
389 wind speeds were calm, i.e., $< 5 \text{ km hr}^{-1}$ (median speed 3.6 km hr^{-1}) and from variable directions,
390 though predominantly from the W and N. The two exceptions were the nights of July 22/23 and
391 August 1/2 when stronger winds ($> 5 \text{ km hr}^{-1}$) from the W and SW persisted. These nights saw
392 relatively high ClNO_2 mixing ratios (see section 3.1.4).

393 The air temperatures were quite mild and ranged from a minimum of $11.0 \text{ }^\circ\text{C}$ to a maximum of
394 $31.9 \text{ }^\circ\text{C}$. The warm temperatures shifted equilibrium K_2 from N_2O_5 towards NO_3 and NO_2
395 (further analyzed in section 3.2.2). At night, temperatures frequently dropped to the dew point,
396 resulting in occasional fog formation (shown as grey rectangles in Figure 3D), sometimes after
397 sunrise. Fog droplets are strong sinks for N_2O_5 (Osthoff et al., 2006). In total, the impact of fog
398 was minor, affecting 5% of the data. In addition, there were two periods with precipitation: The
399 first occurred intermittently on July 20 until the morning of July 21. The second rainfall event
400 was a 24-hour period from mid-day July 22 to the afternoon of July 23 (shown as blue dots in
401 Figure 3D). July 23 also exhibited the highest wind speeds of the campaign (Figure 3C) and
402 lowest daytime photolysis frequencies. The time series of $j(\text{ClNO}_2)$ is shown as a representative
403 example in Figure 3A. The photolysis data indicates that it was sunny on 6 days (July 25, 26,
404 29, Aug 1, 4 and 5) and that the remaining days had variable cloud cover, consistent with hourly
405 meteorological logs that showed 10% of the measurement period affected by precipitation.

406



407



408

409 **Figure 3.** (A) Time series of N_2O_5 and ClNO_2 mixing ratios (left axis) and ClNO_2 photolysis
410 frequency (right axis) observed at T45 near the Abbotsford International Airport. (B) Time
411 series of the ratios of ClNO_2 and N_2O_5 to NO_y (left axis) and of NO_y (right axis). (C) Time
412 series of NO , NO_2 , O_3 , and O_x ($= \text{NO}_2 + \text{O}_3$) mixing ratios. (D) Time series of local wind
413 direction (left axis) and speed (right axis). The blue and grey dots above the time series indicates
414 periods of precipitation (drizzle or rain) and fog, respectively, as identified in hourly
415 meteorological logs.

416

417 3.1.2 NO and NO₂

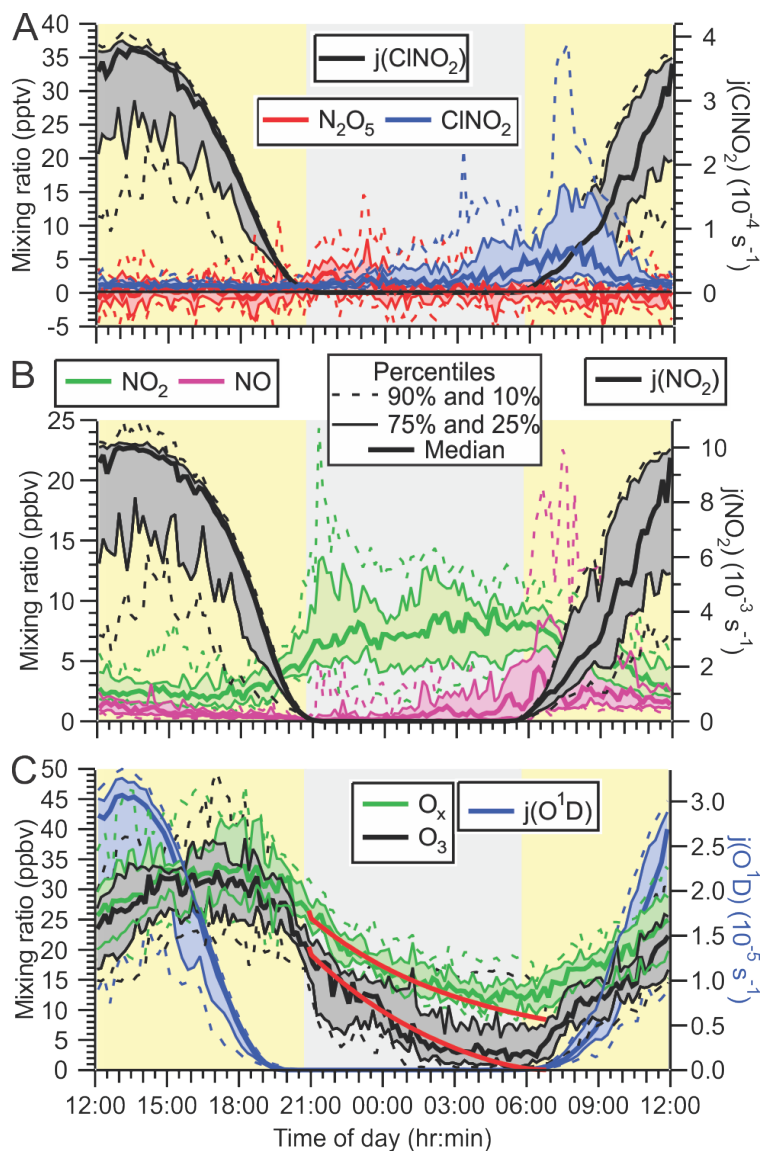
418 The rates of N₂O₅ and ClNO₂ formation depend on the rate of NO₃ production,
419 $P(\text{NO}_3) = k_1[\text{NO}_2][\text{O}_3]$ (analyzed further in section 3.2.2); therefore, it is informative to first
420 examine the mixing ratios of NO₂ and O₃ (see section 3.1.3). The time series of NO, NO₂, O₃,
421 and O_x (= O₃ + NO₂) mixing ratios are shown in Figure 3C, and their diurnal averages are shown
422 as 10th, 25th, 50th, 75th and 90th percentiles in Figures 4B and 4C.

423 The median NO and NO₂ mixing ratios for the entire campaign were 0.9 and 5.9 ppbv,
424 respectively. The average NO_x/NO_y ratio for the entire campaign was 0.89 (data not shown).
425 These concentration levels are characteristic of an urban air mass impacted by relatively fresh
426 emissions from combustion engines in automobiles.

427 At night, mixing ratios of NO were generally lower than during the day though not negligible
428 (median 0.3 ppbv, Figure 4B) as NO was oxidized by O₃ to NO₂ (reaction 8) and was not
429 replenished by NO₂ photolysis. However, mixing ratios of NO increased throughout the night,
430 often coinciding with complete nocturnal removal of O₃ (see section 3.1.3), which indicates the
431 presence of nearby combustion sources of NO_x (most likely automobile exhaust). The presence
432 of NO titrates NO₃ (via reaction 3) and effectively shut down N₂O₅ and ClNO₂ production for
433 most of the study: 68% of the measurement period had NO mixing ratios > 100 pptv and NO₃
434 lifetimes (with respect to its reaction with NO) of < 15 s. In contrast, NO₂ mixing ratios were
435 highest at night (median 7.3 ppbv), amplified further by NO_x emissions that continued
436 throughout the night and likely by low nocturnal mixing heights (see discussion).

437 Mixing ratios of NO and NO_x were highest in the morning hours. Concentration changes at this
438 time of day are difficult to interpret since the NBL breaks up during this time, resulting in
439 vertical mixing of air masses, photolabile species (e.g., ClNO₂, HONO, N₂O₅, etc.) that
440 accumulated overnight begin to photodissociate, and local emissions change with the onset of
441 rush hour.

442 In contrast to the morning increase in NO, an afternoon/early evening maximum in NO was
443 absent. This can be rationalized by a greater abundance of oxidants that oxidize NO to NO₂,
444 i.e., O₃ (see Figures 3 and 4) and organic peroxy radicals in the afternoon, a topic outside the
445 scope of this manuscript.



446

447 **Figure 4.** (A) Diurnal variation of CINO_2 and N_2O_5 mixing ratios (left axis) and CINO_2
448 photolysis frequencies (right axis). (B) Diurnal profiles of NO and NO_2 (left axis) and NO_2
449 photolysis frequency (right axis). (C) Diurnal profiles of O_3 and $\text{O}_x = \text{O}_3 + \text{NO}_2$ (left axis) and
450 $\text{O}_3 \rightarrow \text{O}^1\text{D}$ photolysis frequency (right axis). The superimposed lines shown in red are results
451 from a simple box model (see text).

452

453 3.1.3 O₃ and O_x

454 The time series of O₃ mixing ratios and its diurnal profile are shown in Figure 3C and 4C,
455 respectively. O₃ mixing ratios were small (average ± 1 standard deviation of 16±12 ppbv) and
456 peaked at ~17:00 in the afternoon. The highest concentrations were observed on August 4 from
457 13:55 to 15:30, when mixing ratios were 64.4±1.2 ppbv (the 8-hour running average was 52
458 ppbv). These levels were well below the CAAQS 8-hr standard of 63 ppbv and the 1 hour
459 National Ambient Air Quality Objective of 82 ppbv, smaller than the pre-2003 data analyzed
460 by *Ainslie and Steyn* (2007) and of similar magnitude as observed by a high-density monitoring
461 network in the region in 2012 (Bart et al., 2014).

462 A recurring feature of this data set was the rapid and often complete loss of O₃ at night (Figure
463 4C). This was accompanied by an increase in the NO₂ mixing ratios, though by less (+6 ppbv
464 on average) than the amount of O₃ that was lost (-26 ppbv on average), showing that NO to
465 NO₂ conversion (reaction 8) was a contributor, though minor (~25%) to the nocturnal O₃ loss.

466 The diurnal profile of O_x was similar to that of O₃, in that the highest concentrations occurred
467 in the afternoon (at ~18:00) and a considerable fraction of O_x was removed at night: At sunset,
468 a median amount of 26 ppbv of O_x were present, which decreased to 12 ppbv at sunrise (Figure
469 4C). The pathways contributing to nocturnal O₃ and O_x loss of are probed using box model
470 simulations in section 3.2.1.

471 There were two (out of 16 total) nights when O₃ was not completely removed: on July 22-23
472 and August 1-2, O₃ mixing ratios dropped from a daytime maxima of ~33 ppbv to non-zero
473 nocturnal minima of ~16 ppbv. On both of these nights, ClNO₂ and N₂O₅ mixing ratios were
474 elevated (Figure 3A), and the two largest ClNO₂ to NO_y ratios were observed (Figure 3B). The
475 local wind speeds were > 6 km hr⁻¹, whereas on other nights, local winds were calmer (Figure
476 3C). The greater local wind speeds likely induced more turbulence and a higher vertical mixing
477 height.

478

479 3.1.4 N₂O₅ and ClNO₂

480 Time series of ClNO₂ and N₂O₅ mixing ratios and ClNO₂ photolysis frequencies are shown in
481 Figure 3A. Mixing ratios of ClNO₂ and N₂O₅ were small (campaign averages at night of
482 4.0 pptv and 1.4 pptv, respectively). The mixing ratios peaked prior to sunrise at a median value
483 of 7.9 and 7.8 pptv for ClNO₂ and N₂O₅, respectively. The highest mixing ratio of this campaign
484 was 97 pptv for ClNO₂ and 23 pptv for N₂O₅, both observed on the night of August 1-2. This
485 night was also the only time when nocturnal ClNO₂ mixing ratios exceeded 20 pptv and is
486 analyzed in greater detail in section 3.2.3.

487 Consistent with their low mixing ratios, neither ClNO₂ nor N₂O₅ were significant components
488 of NO_y (Figure 3B): on average, they contributed 0.1% to the nocturnal NO_y budget, though
489 NO_y mixing ratios were large (median 6.3 ppbv at night), typical for a site impacted by urban
490 emissions. The only exception was the night of August 1-2, when ClNO₂ and N₂O₅ constituted
491 2.6% and 1.6% of NO_y, respectively, and NO_y mixing ratios were 4.4 ppbv on average (Figure
492 3B).

493 The ClNO₂ and N₂O₅ mixing ratios are displayed as functions of time of day in Figure 4A.
494 Before midnight local time, N₂O₅ mixing ratios were slightly larger (median value of 1.8 pptv
495 on average) than those of ClNO₂ (median value of 1.4 pptv on average), whereas after midnight,
496 ClNO₂ mixing ratios were larger than those of N₂O₅ (2.0 pptv vs. 0.6 pptv). The latter is
497 consistent with observations at other ground sites, which generally showed higher
498 concentrations of the longer-lived ClNO₂ prior to sunset (Thornton et al., 2010; Mielke et al.,
499 2013). The higher N₂O₅ than ClNO₂ abundances at the beginning of the nights suggests that the
500 N₂O₅ production rate at that time exceeded its ability to react heterogeneously and convert to
501 ClNO₂, potentially due to a lack of available aerosol chloride or otherwise reduced N₂O₅
502 heterogeneous uptake parameters (Thornton et al., 2010).

503 Production of ClNO₂ from N₂O₅ uptake on aerosol ceases after sunrise because of the rapid
504 removal of N₂O₅ and NO₃ as the latter is titrated by NO and destroyed by photolysis (reactions
505 3 and 4) (Wayne et al., 1991). In spite of this, ClNO₂ mixing ratios frequently (on 12 out of 15
506 measurement days) continued to increase after sunrise (Figures 3A and 4), peaking on average
507 at ~07:45 in the morning approximately 2 hours after sunrise. The median mixing ratio at that
508 time was 6.7 pptv larger than the median value of 5.3 pptv observed at sunrise. The most
509 prominent example of this phenomenon occurred on the morning of July 26. For a two hour
510 period leading up to sunrise, there was fog (virtually ensuring the absence of N₂O₅), and ClNO₂



511 mixing ratios were < 5 pptv. The fog then dissipated at sunrise. One hour later, ClNO₂ mixing
512 ratios increased to > 40 pptv. Similar events (though with more modest ClNO₂ increases) were
513 observed on the mornings of July 22, 23, 25, 27, 28, 30, 31, and Aug 1. Two of these (July 23
514 and 27) overlapped with brief fog events.

515 Qualitatively similar ClNO₂ morning peaks have been observed at other ground sites and were
516 rationalized by vertical mixing (Tham et al., 2016; Bannan et al., 2015; Faxon et al., 2015).

517 In the period after the ClNO₂ morning peak after ~09:00, ClNO₂ mixing ratios decreased,
518 coinciding with the increasing ClNO₂ photolysis rate. Box model simulations (see S.I.) indicate
519 that the decay of ClNO₂ (after 09:00) was consistent with its destruction by photolysis.

520 There were two exceptions: the mornings of July 27 and Aug 2, when the decay of ClNO₂
521 concentration occurred at a rate faster than its photolysis. On July 27, fog was not observed
522 until 8:00, at which time the ClNO₂ mixing ratio rapidly decreased because of dissolution and/or
523 an air mass shift to one with a different chemical history. On Aug 2, the campaign maximum
524 of 97 pptv was observed at 04:40 prior to sunrise, followed by a sharp decline. Hourly logs
525 indicated scattered showers at 06:00.

526

527 3.1.5 Aerosol size distribution and composition measurements

528 The time series of submicron surface area density (S_A) observed by the SMPS is shown in
529 Figure 5A. The aerosol loadings were modest: the average (median) surface area density was
530 128 (104) $\mu\text{m}^2 \text{cm}^{-3}$ and ranged from extremes of 26 to $618 \mu\text{m}^2 \text{cm}^{-3}$. Shown on the right hand
531 side is the rate coefficient for heterogeneous uptake of N₂O₅, $k_{\text{N}_2\text{O}_5}$ calculated using equation
532 (10).

$$533 \quad k_{\text{N}_2\text{O}_5} = \frac{1}{4} \gamma \bar{c} S_A \quad (10)$$

534 Here, γ and \bar{c} are the uptake probability and the mean molecular speed of N₂O₅, respectively
535 (Davidovits et al., 2006). For this calculation, a γ value of 0.025 was assumed. The average (± 1
536 standard deviation) of $k_{\text{N}_2\text{O}_5}$ was $1.8 \pm 1.1 \times 10^{-4} \text{ s}^{-1}$.

537 The ACSM submicron aerosol composition data are shown as a time series in Figure 5B and as
538 a function of time of day in Figure 6. Consistent with the size distributions, mass loadings were
539 also modest overall (average $2.3 \mu\text{g m}^{-3}$). The ACSM factor analysis identified oxygenated



540 organic aerosol (OOA) as the largest mass fraction of the non-refractory aerosol (average \pm
541 standard deviation $1.4 \pm 1.2 \mu\text{g m}^{-3}$, 63.3% of the total aerosol mass). Hydrocarbon-like organic
542 aerosol (HOA) associated with primary emissions was a minor component (average
543 $0.03 \mu\text{g m}^{-3}$, 1.1%) but occasionally enhanced in plumes (maximum $8.3 \mu\text{g m}^{-3}$).

544 The oxygenated aerosol fraction (OOA) did not exhibit a discernible diurnal profile (Figure
545 6A), which is consistent with the modest photochemistry at this site as judged from the modest
546 peak O_3 levels observed.

547 The inorganic mass fraction was dominated by nitrate ($0.47 \pm 0.40 \mu\text{g m}^{-3}$, 20.7%). The second
548 most abundant inorganic component was ammonium ($0.2 \pm 1.4 \mu\text{g m}^{-3}$, 8.8%) followed by
549 sulfate ($0.15 \pm 0.15 \mu\text{g m}^{-3}$, 6.8%). The data are of similar magnitude as aerosol mass
550 spectrometry (AMS) data collected at nearby Langley as part of Pacific 2001 (Boudries et al.,
551 2004); then, organics had also been the largest component (average of $1.6 \mu\text{g m}^{-3}$, 49%), though
552 sulfate and ammonium mass loadings had been larger (0.88 and $0.44 \mu\text{g m}^{-3}$, 25% and 14%,
553 respectively) and nitrate mass loadings smaller ($0.38 \mu\text{g m}^{-3}$, 12%).

554 The aerosol was frequently neutralized; the neutralization ratio, $\text{NR} = [\text{NH}_4^+] : ([\text{NO}_3^-] + [\text{SO}_4^{2-}])$
555 was 1.38 (median value). The high NH_3 content is qualitatively consistent with the non-
556 quantitative data collected by Metro Vancouver (using a Thermo Scientific 17i
557 $\text{NH}_3/\text{NO}/\text{NO}_2/\text{NO}_x$ analyzer), which showed large concentrations of gas-phase NH_3 (data not
558 shown).

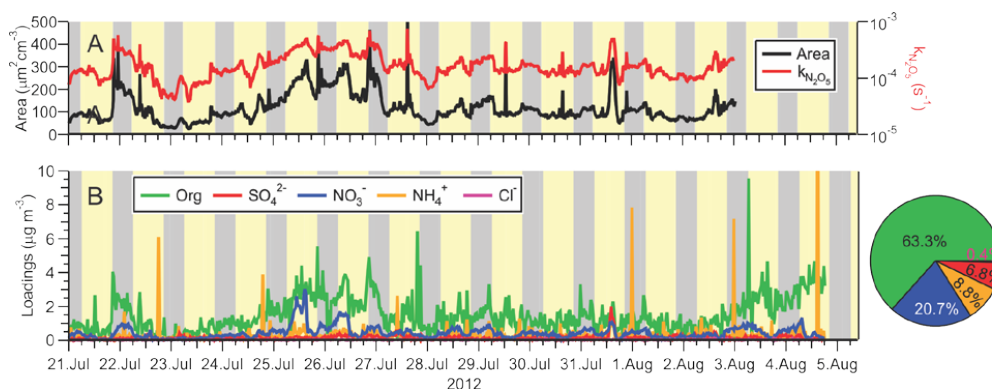
559 The ACSM software also identified chloride with an average (± 1 standard deviation)
560 concentration of $0.01 \pm 0.03 \mu\text{g m}^{-3}$, though it is unclear if this signal was real as it did not vary
561 over the course of the campaign and was below the stated ACSM detection limit of $0.2 \mu\text{g m}^{-3}$
562 (Ng et al., 2011).

563 Aerosol nitrate exhibited a clear diurnal profile with higher concentrations at night (Figure 6B).
564 In particular, the amount of aerosol nitrate increased at the beginning of the night, when the
565 nocturnal NO_3 production rates were greatest.

566 Previous AMS measurements in Vancouver as part of Pacific 2001 reported a slightly higher
567 total mass loadings of $7.0 \mu\text{g m}^{-3}$ that included a greater HOA component ($2.4 \mu\text{g m}^{-3}$, 34%)
568 and a smaller nitrate fraction ($0.6 \mu\text{g m}^{-3}$, 8.5%) (Alfarra et al., 2004; Jimenez et al., 2009) than
569 observed here. The lower HOA in this data set are likely a result of tighter emission controls
570 implemented since the earlier study, a topic outside the scope of this paper.



571

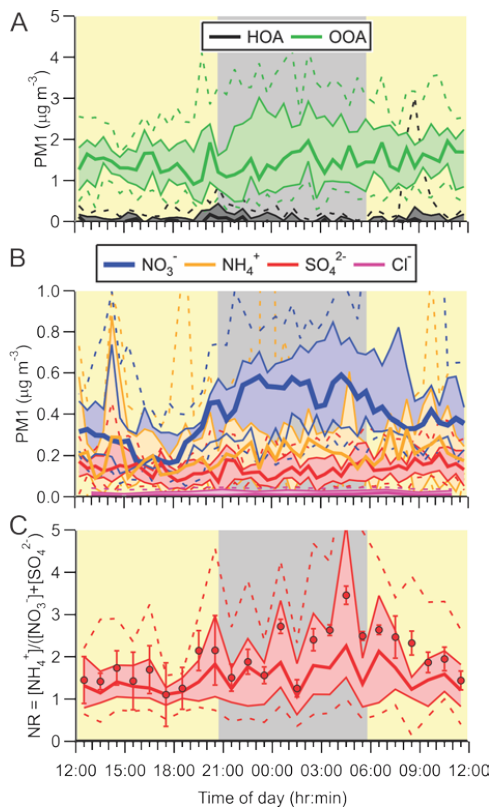


572

573 **Figure 5.** Time series of (A) submicron surface area density measured by the TSI 3034 scanning
574 mobility particle sizer (lhs) and calculate heterogeneous N_2O_5 uptake rate coefficient assuming
575 $\gamma=0.025$ (rhs), and (B) non-refractory submicron aerosol species measured by ACSM. The
576 average total loading was $2.3 \mu\text{g m}^{-3}$. The pie chart shows the average campaign composition.
577



578



579

580 **Figure 6.** Diurnal averages of submicron (PM1) ACMS data. (A). Organic aerosol displayed
581 as hydrocarbon-like organic aerosol (HOA) and oxygenated organic aerosol (OOA). (B)
582 Inorganic aerosol fractions. (C) Neutralization ratio (NR).



583 3.1.6 Hydrocarbon measurements

584 Mixing ratios of hydrocarbons were quantified during daytime and during the nights of August
585 2-3 and 3-4. A portion of the hydrocarbon data is shown in Figure 7A.

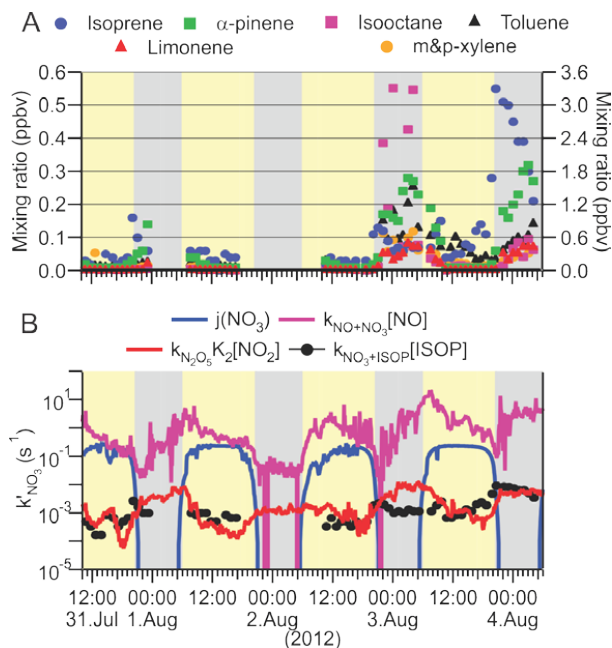
586 Mixing ratios were generally smaller during the day than during night, due to the larger daytime
587 mixing heights. On the nights of August 2/3 and 3/4, N_2O_5 was not detected, consistent with
588 low $\text{P}(\text{NO}_3)$ values as O_3 mixing ratios approached zero (Figure 3). At the same time, there
589 were strong NO_3 sinks present: Mixing ratios of α -pinene and limonene (left-hand axis)
590 increased throughout the night, as thermal emissions continued into the shallow NBL. In
591 contrast, mixing ratios of isoprene, whose emissions are driven by photosynthesis (Hewitt et
592 al., 2011; Guenther et al., 1995), increased at the beginning of the nights and then decreased as
593 isoprene was removed by oxidation with O_3 and NO_3 and by transport. Throughout both nights,
594 the site was also influenced by anthropogenic hydrocarbons (e.g., isooctane and toluene, right-
595 hand axis). Because synoptic conditions as judged from local wind speed and direction (Figure
596 3D) were similar on most of the other nights when hydrocarbons were not quantified, the data
597 shown in Figure 7A were likely representative for much of the campaign.

598 The VOC data were not sufficiently comprehensive to allow an accurate determination of the
599 NO_3 loss frequency to hydrocarbons, given by $\sum_{\text{NO}_3+\text{VOC}_i} [\text{VOC}]_i$. Shown in Figure 7B is the
600 loss frequency of NO_3 to isoprene, calculated by multiplying its concentration with the NO_3
601 rate coefficient taken from *Seinfeld and Pandis* (2006). Loss of NO_3 to isoprene was a small
602 sink compared to its loss to NO via reaction (3) and NO_3 photolysis but is approximately on par
603 with $k_{\text{N}_2\text{O}_5} K_2[\text{NO}_2]$.

604



605



606

607 **Figure 7.** (A) Time series of selected VOC mixing ratios observed on the nights of August
608 2/3 and August 3/4, 2012. Biogenic VOCs (isoprene, α -pinene and limonene) are shown on
609 the left-hand axis, and anthropogenic VOCs (isooctane, toluene and m&p-xylene) on the
610 right-hand axis. The α -pinene and limonene measurements are semiquantitative. (B) Time
611 series of NO_3 loss rate coefficients. ISOP = isoprene.

612



613 **3.2 Analysis**

614 **3.2.1 Box model simulations of the nocturnal O₃ and O_x loss in the NBL**

615 In initial simulations, the O₃ and NO₂ deposition rates were tuned until the median nocturnal
616 O_x loss was reproduced. An O₃ dry deposition rate of $4 \times 10^{-5} \text{ s}^{-1}$ produced a simulation that
617 reasonably matched the observations (Figure S-1). The magnitude of this rate corresponds to a
618 NBL height of 50 m, the same mixing height that was frequently observed in balloon vertical
619 profiles reported by Pisano et al. (1997). Modeling studies have assumed N₂O₅ and NO₃
620 deposition velocities of up to 2 cm s^{-1} in urban areas (Sander and Crutzen, 1996); adopting this
621 value allows the dry deposition rate constants of N₂O₅ and NO₃ to be estimated at $\sim 4 \times 10^{-4} \text{ s}^{-1}$,
622 which is on par with the estimated heterogeneous uptake rate constant of N₂O₅ on submicron
623 aerosol.

624 Next, the generic biogenic VOC was added. For this, a biogenic hydrocarbon abundance of
625 1 ppbv at sunset (mostly isoprene – see Figure 7) and a (monoterpene) emission rate of 3×10^5
626 molecules $\text{cm}^{-3} \text{ s}^{-1}$ based on the crop emission factor given by Guenther et al. (2012) into a 50 m
627 deep NBL were assumed. This assumed flux gives a similar emission rate as the 0.3 ppbv
628 increase over a 6 hour period observed on Aug 3-4 (Figure 7).

629 The addition of this biogenic VOC only had a marginal effect on O_x and resulted in a slightly
630 better reproduction of the faster O_x loss at the beginning of the night (not shown).

631 The simulations presented in Figures S-1 underpredict the observed loss of O₃, necessitating
632 the addition of an NO source that results in selective removal of O₃ while preserving O_x. Since
633 automobiles are the largest NO_x source in the region, a constant emission source of 95% NO
634 and 5% NO₂ (Wild et al., 2017) was added and its magnitude varied. The NO_x source strength
635 necessary to reproduce the median O₃ loss was $\sim 1.1 \text{ ppbv hr}^{-1}$. The simulation results using
636 these parameters are superimposed (in red) in Figure 4C. There is reasonable agreement
637 between the simulation and observations until $\sim 3:00$, which shows that the nocturnal O₃ and O_x
638 loss can be rationalized without active NO₃ and N₂O₅ chemistry and suggests that NO₃, N₂O₅,
639 and ClNO₂ did not contribute significantly to O_x and O₃ loss in the NBL.

640



641 3.2.2 Metrics of nocturnal nitrogen oxide chemistry: $P(\text{NO}_3)$, $\phi'(\text{ClNO}_2)$ and
642 $\tau(\text{N}_2\text{O}_5)$

643 Nocturnal N_2O_5 chemistry was analyzed using several common metrics: the rate of NO_3
644 production by reaction (1), $P(\text{NO}_3)=k_1[\text{NO}_2][\text{O}_3]$, the yield of ClNO_2 relative to the total amount
645 of NO_3 formed at night, $\phi'(\text{ClNO}_2)$, and the steady state lifetime of N_2O_5 , $\tau(\text{N}_2\text{O}_5)$.

646 The time of day dependence of $P(\text{NO}_3)$ is shown in Figure 8A. The NO_3 production rates were
647 small (median values < 0.3 ppbv hr^{-1}) and were larger during the day than at night due to the
648 low O_3 mixing ratios. After midnight, for example, the median $P(\text{NO}_3)$ was (55 ± 23) pptv hr^{-1} .
649 These are very modest NO_3 production rates for a site influenced by urban emissions. In a recent
650 study on a mountain top in Hong Kong, for instance, $P(\text{NO}_3)$ in excess of 1 ppbv hr^{-1} was
651 observed in polluted air (Brown et al., 2016).

652 The median integrated nocturnal NO_3 production over the course of the night was 940 pptv
653 (Figure 8A, right hand axis), of which 600 pptv were produced before midnight.

654 The amount of ClNO_2 produced relative to this amount, $\phi'(\text{ClNO}_2)$, was very small (median
655 0.17%, maximum 5.4% on the morning of August 2) and considerably less than reported by our
656 group for Calgary (median 1.0%) (Mielke et al., 2016) and Pasadena, CA (median 12%)
657 (Mielke et al., 2013).

658 A frequently calculated metric of nighttime nitrogen oxide chemistry are the steady state
659 lifetimes of NO_3 and N_2O_5 , $\tau(\text{NO}_3)$ and $\tau(\text{N}_2\text{O}_5)$ (Aldener et al., 2006; Heintz et al., 1996). The
660 latter is calculated from (Brown et al., 2003; Brown and Stutz, 2012):

$$661 \quad \tau(\text{N}_2\text{O}_5) = \frac{[\text{N}_2\text{O}_5]}{P(\text{NO}_3)} = \frac{[\text{N}_2\text{O}_5]}{k_1[\text{NO}_2][\text{O}_3]} \approx \left(k_{\text{N}_2\text{O}_5} + \frac{k_{\text{NO}_3}}{K_2[\text{NO}_2]} \right)^{-1} \quad (11)$$

662 Here, $k_{\text{N}_2\text{O}_5}$ and k_{NO_3} are the pseudo-first order loss-rate coefficients of N_2O_5 and NO_3
663 respectively, and K_2 is the equilibrium constant for equilibrium (2).

664 The derivation of equation (11) is given by *Brown et al.* (2003). A central assumption in this
665 derivation is that NO_3 , NO_2 , and N_2O_5 more rapidly equilibrate than NO_3 is formed and either
666 NO_3 or N_2O_5 are destroyed, i.e., $\text{NO}_3+\text{N}_2\text{O}_5$ are assumed to be in steady state with respect to
667 production and loss. *Brown et al.* (2003) outlined potential pitfalls concerning the validity of
668 the steady state approximation and recommended that box model simulations are carried out to



669 evaluate if a steady state in N_2O_5 can be assumed. Using the median nocturnal NO_2 and O_3
 670 mixing ratios of 7.5 ppbv and 18 to 5.0 ppbv, respectively, a temperature of 286 K, and assumed
 671 N_2O_5 and NO_3 pseudo-first order loss frequencies of $1 \times 10^{-3} \text{ s}^{-1}$ and between $1 \times 10^{-2} \text{ s}^{-1}$ and 0 s^{-1} ,
 672 the time to achieve steady state in N_2O_5 is 70 min or less (data not shown). Thus, the steady
 673 state assumption is reasonable for this data set.

674 A key parameter in equation 11 is the strongly temperature dependent equilibrium constant K_2
 675 (Osthoff et al., 2007). At night, the air temperatures during this study were quite warm (median
 676 nocturnal minimum of +13 °C) and did not vary a lot between nights (Figure 8B). The warm
 677 temperatures shift equilibrium 2 away from N_2O_5 and towards NO_3 and NO_2 , making losses via
 678 NO_3 (reactions 3-4 and 7) more competitive with the losses of N_2O_5 (that produce ClNO_2), i.e.,

679 the $\frac{k_{\text{NO}_3}}{K_2[\text{NO}_2]}$ term in equation 11 becomes large relative to $k_{\text{N}_2\text{O}_5}$. On the other hand, the

680 relatively high NO_2 mixing ratios (median value 7.5 ± 0.8 ppbv) shift the equilibrium towards
 681 N_2O_5 . Thus, in spite of the relatively warm temperatures, the $\text{N}_2\text{O}_5:\text{NO}_3$ equilibrium ratios were
 682 large on aggregate (>15 ; Figure 8B), enabling ClNO_2 formation via reaction 7.

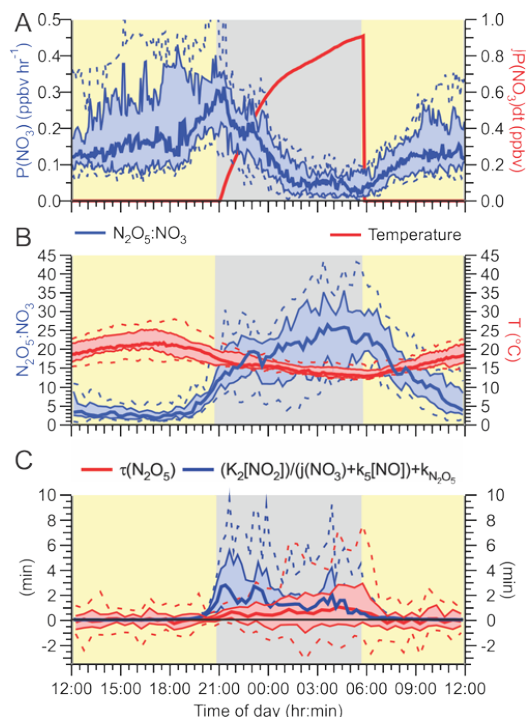
683 The steady state lifetime of N_2O_5 , $\tau(\text{N}_2\text{O}_5)$, is shown as a diurnal average in Figure 8C. The
 684 median $\tau(\text{N}_2\text{O}_5)$ at night was short (~ 1 min), and the 90th percentile peaked at a modest 7.6 min
 685 at sunrise, considerably shorter than observed above the NBL (Brown et al., 2006b) and at other
 686 ground sites (Wood et al., 2005; Crowley et al., 2010; Brown et al., 2016)

687 Superimposed on the right-hand side of Figure 8C are upper limits to the steady state lifetime
 688 of N_2O_5 calculated using the titration of NO_3 by NO (reaction 3), NO_3 photolysis (reaction 4),
 689 and N_2O_5 heterogeneous uptake calculated using equation 10, all divided by the N_2O_5 over NO_3
 690 ratio at equilibrium, given by $K_2\text{NO}_2$ (Figure 8B).

$$691 \quad \tau(\text{N}_2\text{O}_5) = \left(\frac{k_{\text{NO}_3}}{K_2[\text{NO}_2]} + k_{\text{N}_2\text{O}_5} \right)^{-1} < \left(\frac{k_3[\text{NO}] + j(\text{NO}_3)}{K_2[\text{NO}_2]} + k_{\text{N}_2\text{O}_5} \right)^{-1} \quad (12)$$

692 Missing from equation (12) are losses of NO_3 to hydrocarbons (which was omitted because of
 693 the poor VOC data coverage) and terms for NO_3 and N_2O_5 dry and wet (i.e., on cloud and rain
 694 droplets) deposition.

695



696

697 **Figure 8.** (A) NO_3 production rate $P(\text{NO}_3) = k_1[\text{NO}_2][\text{O}_3]$ as a function of time of day. The red
 698 line is the total amount NO_3 generated since sunset, $\int P(\text{NO}_3)dt$. (B) Equilibrium ratio of N_2O_5
 699 to NO_3 calculated by multiplying the temperature-dependent equilibrium constant, K_2 , with the
 700 NO_2 concentration, $[\text{NO}_2]$ (left axis), and air temperature (right axis). (C) Steady state lifetime
 701 of N_2O_5 (left axis) and upper limits calculated using equation (12) (right axis) as functions of
 702 time of day.

703

704 The median "observed" $\tau(\text{N}_2\text{O}_5)$ is below or equal to the upper limit calculation with equation
 705 12 during both night and day. The largest discrepancy is observed at the beginning of the night,
 706 when oxidation of (unsaturated) hydrocarbons by NO_3 (reaction 6) was likely most significant
 707 due to the presence of isoprene. It is also the time when the steady state approximation is most
 708 likely invalid.

709

710 3.2.3 Heterogeneous conversion of N₂O₅ to ClNO₂ on the night of August 1/2

711 Phillips et al. (2016) recently applied several methods to estimate the N₂O₅ uptake parameter
712 (γ) and yield of ClNO₂ (ϕ) from ambient measurements of NO₃, N₂O₅, ClNO₂, and aerosol
713 nitrate. One of these methods uses the covariance of ClNO₂ and aerosol nitrate production rates,
714 P(NO₃⁻) and P(ClNO₂):

$$715 \quad \phi = 2(P(\text{NO}_3^-)/P(\text{ClNO}_2) + 1)^{-1} \quad (15)$$

$$716 \quad \gamma = 2(P(\text{NO}_3^-) + P(\text{ClNO}_2)) / (c S_A [\text{N}_2\text{O}_5]) \quad (16)$$

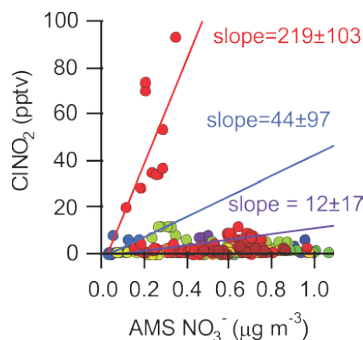
717 In the above equation, c is the mean molecular speed of N₂O₅ ($\approx 237 \text{ m s}^{-1}$). The use of equations
718 (15-16) assumes that the relevant properties of the air mass are conserved (i.e., identical upwind
719 of and at the measurement location and affected identically by air masses mixing), that losses
720 of measured species are not significant, that the efficiency of N₂O₅ uptake and production of
721 ClNO₂ and NO₃⁻ is independent of particle size, and the absence of partitioning of HNO_{3(g)} and
722 aerosol nitrate between the gas and particle phases (Phillips et al., 2016). It is assumed further
723 that production of nitrate on refractory aerosol (that the ACMS does not quantify) is minimal.

724 In this data set, ClNO₂ and submicron aerosol nitrate rarely covaried (Figure 9); the only
725 instance showing a modest correlation ($r=0.66$) is the time period prior to sunrise of August 2
726 (shown as red dots in Figure 9).

727



728



729

730 **Figure 9.** Scatter plot of ClNO_2 mixing ratios with submicron (PM_1) ACMS NO_3^- data. The
731 slopes were calculated for three periods: Aug 2, 01:25 – 04:55 (red dots; slope = 219 ± 103 ; $\phi =$
732 0.72), July 23, 03:00 – 04:25 (blue dots slope = 44 ± 97 ; $\phi = 0.21$), and July 21, 02:25 – 05:20
733 (purple dots slope = 12 ± 17 ; $\phi = 0.06$).

734

735 The night of August 1-2 exhibited the highest nocturnal nitrogen oxide concentrations for the
736 entire campaign. Winds were initially from the NW and relatively light ($4.8 \pm 0.7 \text{ km hr}^{-1}$) and
737 after 01:00 picked up in speed (to $8.2 \pm 1.3 \text{ km hr}^{-1}$) and shifted to the W. Judging from the
738 HYbrid Single-Particle Lagrangian Integrated Trajectory (HYSPLIT) back trajectories (Draxler
739 and Rolph, 2013), the upwind air had moved in from the coast, roughly from the direction of
740 the city of Victoria, BC (Odam-Ankrah, 2015).

741 After sunset at $\sim 21:00$ local time, N_2O_5 levels started increasing and continued to increase until
742 about 01:30 (Figure 3A). The steady state N_2O_5 lifetime at this time was the highest of the
743 campaign, ~ 10 min. At 01:20, ClNO_2 mixing ratio increased from 20.4 pptv at 01:25 to
744 93.7 pptv at 04:55 and the aerosol nitrate content from 0.10 to $0.34 \mu\text{g m}^{-3}$ (40 to 127 pptv).
745 During this time, N_2O_5 mixing ratios and PM_1 surface area density were relatively constant,
746 11.1 ± 6.4 pptv and $67 \pm 4 \mu\text{g m}^{-3}$ (average \pm standard deviation), respectively. The combined
747 amount of N_2O_5 , ClNO_2 and NO_3^- produced (172 pptv) is less than the amount of NO_3^- produced
748 from reaction (1) which was 519 pptv during this period.

749 From equations (15) and (16), a ClNO_2 yield of $\phi = 0.72 \pm 0.34$ and an N_2O_5 uptake probability
750 of $\gamma = 0.15 \pm 0.07$ were calculated for this period. Both of these values are upper limits because



751 production of ClNO₂ from uptake of N₂O₅ on unquantified supermicron (i.e., > 0.5 μm) or
752 refractory aerosol (which takes place simultaneously) is not accounted for.

753 A γ value of > 0.05 is greater than can be rationalized from laboratory and field studies (Chang
754 et al., 2011) and is hence unrealistic. This suggests that ClNO₂ production took place
755 predominantly on supermicron or refractory aerosol, which likely was comprised of mainly sea
756 salt derived aerosol on this night.

757 On the other hand, if one assumes that all of the ClNO₂ is produced on supermicron or refractory
758 aerosol such that P(ClNO₂) on submicron aerosol equals 0 pptv s⁻¹ (which is not unreasonable
759 considering the absence of measurable amounts of aerosol chloride in this size fraction, see
760 section 3.1.5), a γ value of 0.08±0.04 is calculated. This large value suggests very efficient
761 N₂O₅ uptake (and conversion to aerosol nitrate) on the non-refractory submicron aerosol that
762 night.

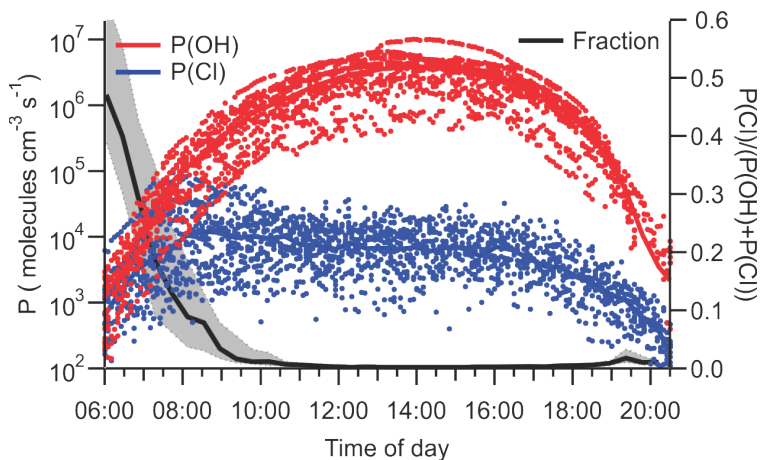
763

764 3.3 Impacts of ClNO₂ on radical production

765 Photolysis of ClNO₂ increases the rates of photochemical O₃ production (and hence worsen air
766 quality) by producing NO₂ and reactive Cl atoms (reaction 6). The amounts of ClNO₂ available
767 for photolysis in the morning (median 3.5 pptv at sunrise and 6.8 pptv at 08:00 local time) were
768 too small to have had a measurable impact on local NO₂ concentrations (Figure 3C) but were
769 sufficiently large to, at least occasionally, impact radical budgets.

770 Figure 10 shows the instantaneous radical production rates of Cl and OH,
771 $P(\text{Cl})=j(\text{ClNO}_2)\times[\text{ClNO}_2]$ and P(OH) from reaction of O(¹D)+H₂O. The latter was calculated
772 from an assumed steady state in O(¹D) with respect to its production from O₃ photolysis and
773 reactions with N₂, O₂, and H₂O as described by *Mielke et al.* (2016). This analysis does not
774 account for OH radical production from photolysis of nitrous acid or aldehydes and, hence,
775 overestimates the importance of Cl radicals.

776



777

778 **Figure 10.** Plots of instantaneous rates of Cl (blue) and OH (red) radical production from ClNO_2
779 photolysis and reaction of O^1D , generated from O_3 photolysis, with H_2O and as a function of
780 time of day. The fraction of radicals produced from ClNO_2 photolysis is shown in black. The
781 solid line indicates median values, and shaded areas the 75th and 25th percentiles.

782

783 The largest $P(\text{Cl})$ values were observed on July 26, 07:45 local time (9.5×10^4 atoms $\text{cm}^{-3} \text{s}^{-1}$),
784 accounting for 40% of the total radical production. The largest fraction of radicals produced
785 from ClNO_2 photolysis was observed on the same day at 6:35 local time (74%, 7.8×10^3 atoms
786 $\text{cm}^{-3} \text{s}^{-1}$). The photolysis of ClNO_2 produces a median value of 6.5×10^3 atoms $\text{cm}^{-3} \text{s}^{-1}$ during
787 daytime, which is negligibly small compared to the median $P(\text{OH})$ of 3.8×10^6 molecules cm^{-3}
788 s^{-1} at noon.

789

790 **4 Discussion**

791 It is now well-established that ClNO₂ is an abundant nitrogen oxide in many regions of the
792 troposphere (Table 3). The results presented in this paper are atypical in that they show
793 consistently small ClNO₂ mixing ratios in spite of close proximity to sources, i.e., in a region
794 where nearby oceanic emissions of sea salt aerosol and NO_x emissions from a megacity
795 combine. In the following, factors contributing to the low ClNO₂ mixing ratios observed in this
796 study and broader implications of ClNO₂ in the LFV are discussed.

797 The main reason for the low ClNO₂ mixing ratios observed in this work are the low nocturnal
798 mixing ratios of O₃ and small NO₃ production rate, P(NO₃), resulting from the stratification of
799 the boundary layer at night and decoupling of the shallow NBL from the NRL. In the following,
800 it is assumed that a boundary layer structure similar to those observed during PACIFIC 93
801 (Pisano et al., 1997; McKendry et al., 1997; Hayden et al., 1997) also existed on most
802 measurement nights of this study. Once the nocturnal boundary layer formed at sunset, O₃ and
803 O_x in the NBL were rapidly (lifetime of ~ 4 hours) removed. The box model simulations
804 presented in section 3.2.1 show that this removal can be rationalized by dry deposition and
805 titration of O₃ with NO and biogenic VOCs alone, leaving little room for nitrogen oxide
806 chemistry to destroy O₃ or NO₂, for example, via heterogeneous formation of HONO which
807 destroys NO₂ (Bröske et al., 2003; Stutz et al., 2004a; Indarto, 2012) or formation of N₂O₅ and
808 subsequent heterogeneous hydrolysis which consumes 2 molecules of NO₂ and 1 molecule of
809 O₃ (Brown et al., 2006a). It is the often complete absence of O₃ at night which distinguishes
810 this data set from the other measurement locations for which ClNO₂ data have been reported,
811 including continental sites where aerosol chloride is likely less abundant (Table 3).

812 A compounding factor in this study was the occasional formation of fog and occasional
813 precipitation events. Fog droplets act as a very rapid sink for NO₃ and N₂O₅ (Osthoff et al.,
814 2006), which shuts down ClNO₂ production, and may have also directly contributed
815 episodically to ClNO₂ losses, for example on the morning of July 27. Overall, though, the
816 contribution of fog to ClNO₂ losses in this data set was minor, as only 5% of the measurement
817 period was impacted by fog. However, this potential ClNO₂ loss mechanism should be
818 investigated further in future lab studies.

819 The rapid drop of ClNO₂ mixing ratio at around 06:00 of Aug 2 is interesting in that it coincided
820 with a very brief precipitation event. Though an air mass shift cannot be ruled out, this
821 coincidence suggests the possibility that scavenging of ClNO₂ by rain droplets followed by



822 hydrolysis may be a possible loss pathway. Scavenging of NO_3 , N_2O_5 , and ClNO_2 by rain
823 droplets is currently not constrained by laboratory investigations (unlike other gases, such as
824 SO_2 or NH_3 (Hannemann et al., 1995)). Similarly to fog, precipitation was not a major factor in
825 this data set as it affected only 10% but may be in other locations or seasons that experience
826 higher rainfall amounts.

827 An important observation is the lack of non-refractory submicron aerosol chloride (Figure 5B).
828 This suggests that there was limited redistribution of chloride from acidification of sea salt
829 aerosol onto other aerosol surfaces in this data set. Such a redistribution was observed, for
830 example, during the Calnex-LA campaign (Mielke et al., 2013). This in turn implies that the
831 submicron aerosol surface did not significantly participate in the production of ClNO_2 from
832 N_2O_5 uptake in the NBL, broadly consistent with the conclusions in section 3.2.3.

833 The low observed $\tau(\text{N}_2\text{O}_5)$ levels are consistent with earlier studies that reported strong vertical
834 gradients in $\tau(\text{N}_2\text{O}_5)$ due to elevated near-surface sinks from emissions by plants (i.e.,
835 monoterpenes) and automobiles (i.e., NO and butadiene (Curren et al., 2006)) that titrate NO_3
836 (Stutz et al., 2004b; Wang et al., 2006; Brown et al., 2007; Young et al., 2012). An emblematic
837 example is the study by Wood *et al.* at a ground site east of the San Francisco Bay Area in
838 January 2004: They observed relatively modest N_2O_5 mixing ratios of up to 200 pptv,
839 corresponding to $\tau(\text{N}_2\text{O}_5) < 5$ min for the entire study period (Wood et al., 2005). Studies for
840 which vertically resolved data were available (e.g., (Stutz et al., 2004b; Wang et al., 2006;
841 Brown et al., 2007; Young et al., 2012; Tsai et al., 2014) generally showed higher N_2O_5
842 concentrations and hence larger $\tau(\text{N}_2\text{O}_5)$ aloft in the NRL than at the surface.

843 A different scenario likely played out aloft in the NRL, which would exhibit higher NO_3
844 production rates (via reactions 1) than the surface layer. Assuming levels of 20 ppbv of O_3 and
845 NO_2 in the NRL (Pisano et al., 1997; McKendry et al., 1997), the NO_3 production rate would
846 equal ~ 1.1 ppbv hr^{-1} in the NRL, roughly on par with values recently reported for Hong Kong,
847 the current record holder for ClNO_2 mixing ratios (Brown et al., 2016; Wang et al., 2016).
848 Recent aircraft and tower studies have shown high rates of production of ClNO_2 aloft (Riedel
849 et al., 2013; Young et al., 2012), which likely also occurred in this work.

850 In contrast, the low mixing height of the NBL is conducive to high levels of biogenic
851 hydrocarbons (section 3.1.6). The nocturnal temperatures during this study were quite warm
852 and did not vary a lot between nights (Figure 8B). Emissions of monoterpenes, which are
853 reactive towards NO_3 , are driven by a temperature-dependent process from storage tissue within



854 the plants at night (Guenther et al., 1995) and, hence, were likely substantial. Their presence is
855 likely responsible for some of the gap between the low "observed" N_2O_5 steady lifetimes,
856 $\tau(\text{N}_2\text{O}_5)$, compared to the upper limit set by reactions 3-4. Even if one assumes a relatively large
857 uptake probability of $\gamma=0.025$ and accounts for the large ratios of $\text{N}_2\text{O}_5:\text{NO}_3$, the loss rate of
858 N_2O_5 on submicron aerosol was likely small in comparison to losses via NO_3 for most of this
859 data set (Figure 7B). Hence, only a small fraction of the integrated nocturnal NO_3 production
860 of 940 pptv resulted in ClNO_2 formation at the surface.

861 Because of the relatively long lifetime of ClNO_2 , the breakdown of the surface layer and
862 merging of the surface air with the NRL constituted itself as a ClNO_2 "morning peak" in a
863 similar manner as what has recently been reported at other locations (Tham et al., 2016; Bannan
864 et al., 2015; Faxon et al., 2015). This morning peak is rationalized by higher net ClNO_2
865 production in the NRL; the break-up of this layer ~2 hours after sunrise then mixes ClNO_2 down
866 to the surface. Such a vertical mixing process was not seen during Calnex-LA (Young et al.,
867 2012; Tsai et al., 2014) where the NBL was sufficiently deep to prevent complete O_3 removal
868 and the ClNO_2 produced mixed down to the surface at night.

869 Assuming a 100 m deep NRL where ClNO_2 production takes place, a mixed layer height of
870 500 m by 08:00 (Pisano et al., 1997) and negligible destruction of ClNO_2 by photolysis (which
871 is reasonable as the lifetime of ClNO_2 with respect to photolysis is >4.6 hours at that time of
872 day), a morning increase in ClNO_2 mixing ratio by 40 pptv at the surface as seen on the morning
873 of July 26 suggests a pool of ClNO_2 in the NRL at sunrise of ~200 pptv, likely a modest value
874 considering that the (assumed) NO_3 production rate may have integrated to ~9 ppbv over the
875 course of the night.

876 The largest nocturnal ClNO_2 mixing ratios were observed on July 22/23 and August 1/2. Both
877 of these nights exhibited high wind speeds and are counterexamples to what was observed on
878 other nights. We speculate that the higher levels of wind shear and turbulence altered the
879 nocturnal boundary layer structure which exhibited a greater degree of vertical mixing and
880 higher O_3 concentrations at the surface. Consistent with this interpretation and the notion that
881 an isolated NRL with higher net ClNO_2 production was absent on those nights, the mornings of
882 July 23 and Aug 2 did not show a "morning peak". In contrast, low surface wind speeds were
883 observed on the other nights, facilitating a stable and shallow nocturnal surface layer.

884 It is conceivable that a land-sea breeze effect transported air from a region closer to the coast
885 that saw higher ClNO_2 production than at Abbotsford, i.e., that the ClNO_2 morning peaks are



886 generated by horizontal as opposed to vertical transport. Large NO_3 mixing ratios have been
887 reported at Saturna Island, which strongly suggest that sizeable reservoirs of ClNO_2 form
888 offshore at night. However, it is known how far inland these reservoirs extend. Considering the
889 average wind speed in the morning (6 km hr^{-1}), distance to the coast (35 km), and close
890 proximity (200 m) of the site to the bottom of the polluted NRL with documented high nocturnal
891 pollution levels and early morning down mixing events, the vertical transport explanation is
892 much more likely correct. Nevertheless, measurements of ClNO_2 at a site closer to the coast
893 (e.g., at White Rock) would be beneficial.

894 Formation of ClNO_2 affects air quality through its photolysis which generates O_x , NO_x , and
895 reactive Cl radicals in the morning, leading to higher net photochemical O_3 production (Sarwar
896 et al., 2014). In spite of the low levels of ClNO_2 observed in this work, the production of radicals
897 from its photodissociation was not always negligible (Figure 10). Conditions leading to O_3
898 exceedances did not develop during this study. If such conditions had developed, it is highly
899 likely that this radical generation would have played a much greater role.

900 The data presented here suggest that higher rates of ClNO_2 and subsequent radical generation
901 take place routinely in layers aloft, processes that are not directly observable at the surface but
902 whose implications are felt as the ultimate product, O_3 , is sufficiently long-lived to mix down
903 to the surface (McKendry et al., 1997). Future studies should therefore target the NRL, for
904 example through missed-approaches by aircraft, a blimp, or from a tall tower, especially during
905 episodes of a developing O_3 exceedance event.

906



907 **5 Summary and conclusions**

908 In this paper, we have presented the first measurements of ClNO₂ and N₂O₅ mixing ratios in
909 the LFV. In spite of the close proximity to NO_x (megacity of Vancouver) and sea salt aerosol
910 (the Pacific Ocean) sources, ClNO₂ and N₂O₅ mixing ratios were small (maximum of 97 and
911 27 pptv, respectively) and smaller than observed at other measurement locations for which
912 ClNO₂ abundances were reported. The low mixing ratios are explained through the removal of
913 O₃ by deposition and titration with NO in a shallow nocturnal surface layer. Measurements of
914 submicron aerosol composition by ACMS showed no enhancements of particle-phase chloride,
915 which is in contrast to locations where high ClNO₂ mixing ratios were observed (such as
916 Pasadena (Mielke et al., 2013)) and indicates that there was little processing and redistribution
917 of sea salt derived chloride at this location. There is indirect evidence that higher production of
918 ClNO₂ took place above the measurement site in the NRL, observed via downmixing after the
919 break-up of the NBL in the morning, and highlights the need for future vertically resolved
920 measurements (e.g., from an aircraft platform) of ClNO₂ and N₂O₅ mixing ratios in the LFV.
921 Conditions leading to O₃ exceedences did not develop during the relatively short measurement
922 period of 2 weeks, such that the full impact that nocturnal formation of ClNO₂ could have on
923 radical production and NO₂ recycling remains unquantified.

924



925 **Data availability**

926 The data used in this study are available from the corresponding author upon request
927 (hosthoff@ucalgary.ca).

928

929 **Acknowledgments**

930 This project was undertaken with the financial support of the Government of Canada through
931 the Federal Department of the Environment. Ce projet a été réalisé avec l'appui financier du
932 Gouvernement du Canada agissant par l'entremise du ministère fédéral de l'Environnement.
933 Partial funding for this work was provided by the Natural Sciences and Engineering Research
934 Council of Canada (NSERC) in the form of operating ("Discovery") and Research Tools and
935 Instruments (RTI) grants. The Abbotsford field study was financially supported by a BC Clear
936 research grant from the Fraser Basin Council of British Columbia and by Metro Vancouver.

937

938



939 **References**

- 940 Ainslie, B., Steyn, D. G., Reuten, C., and Jackson, P. L.: A Retrospective Analysis of Ozone
941 Formation in the Lower Fraser Valley, British Columbia, Canada. Part II: Influence of
942 Emissions Reductions on Ozone Formation, *Atmosphere-Ocean*, 51, 170-186,
943 10.1080/07055900.2013.782264, 2013.
- 944 Aldener, M., Brown, S. S., Stark, H., Williams, E. J., Lerner, B. M., Kuster, W. C., Goldan, P.
945 D., Quinn, P. K., Bates, T. S., Fehsenfeld, F. C., and Ravishankara, A. R.: Reactivity and loss
946 mechanisms of NO_3 and N_2O_5 in a polluted marine environment: Results from in situ
947 measurements during New England Air Quality Study 2002, *J. Geophys. Res.*, 111, D23S73,
948 doi:10.1029/2006JD007252, 2006.
- 949 Alfarra, M. R., Coe, H., Allan, J. D., Bower, K. N., Boudries, H., Canagaratna, M. R., Jimenez,
950 J. L., Jayne, J. T., Garforth, A. A., Li, S.-M., and Worsnop, D. R.: Characterization of urban
951 and rural organic particulate in the Lower Fraser Valley using two Aerodyne Aerosol Mass
952 Spectrometers, *Atmos. Environ.*, 38, 5745-5758, 10.1016/j.atmosenv.2004.01.054, 2004.
- 953 Alicke, B., Geyer, A., Hofzumahaus, A., Holland, F., Konrad, S., Patz, H. W., Schafer, J., Stutz,
954 J., Volz-Thomas, A., and Platt, U.: OH formation by HONO photolysis during the BERLIOZ
955 experiment, *J. Geophys. Res.*, 108, 8247, 10.1029/2001JD000579, 2003.
- 956 Bannan, T. J., Booth, A. M., Bacak, A., Muller, J. B. A., Leather, K. E., Le Breton, M., Jones,
957 B., Young, D., Coe, H., Allan, J., Visser, S., Slowik, J. G., Furger, M., Prévôt, A. S. H., Lee, J.,
958 Dunmore, R. E., Hopkins, J. R., Hamilton, J. F., Lewis, A. C., Whalley, L. K., Sharp, T., Stone,
959 D., Heard, D. E., Fleming, Z. L., Leigh, R., Shallcross, D. E., and Percival, C. J.: The first UK
960 measurements of nitryl chloride using a chemical ionization mass spectrometer in central
961 London in the summer of 2012, and an investigation of the role of Cl atom oxidation, *J.*
962 *Geophys. Res.*, 120, 5638-5657, 10.1002/2014jd022629, 2015.



- 963 Bart, M., Williams, D. E., Ainslie, B., McKendry, I., Salmond, J., Grange, S. K., Alavi-
964 Shoshtari, M., Steyn, D., and Henshaw, G. S.: High Density Ozone Monitoring Using Gas
965 Sensitive Semi-Conductor Sensors in the Lower Fraser Valley, British Columbia, Environm.
966 Sci. Technol., 48, 3970-3977, 10.1021/es404610t, 2014.
- 967 Behnke, W., George, C., Scheer, V., and Zetzsch, C.: Production and decay of ClNO₂, from the
968 reaction of gaseous N₂O₅ with NaCl solution: Bulk and aerosol experiments, J. Geophys. Res.,
969 102, 3795-3804, 10.1029/96JD03057 1997.
- 970 Bertram, T. H., and Thornton, J. A.: Toward a general parameterization of N₂O₅ reactivity on
971 aqueous particles: the competing effects of particle liquid water, nitrate and chloride, Atmos.
972 Chem. Phys., 9, 8351-8363, 10.5194/acp-9-8351-2009, 2009.
- 973 Biesenthal, T. A., Wu, Q., Shepson, P. B., Wiebe, H. A., Anlauf, K. G., and Mackay, G. I.: A
974 study of relationships between isoprene, its oxidation products, and ozone, in the Lower Fraser
975 Valley, BC, Atmos. Environm., 31, 2049-2058, 10.1016/S1352-2310(96)00318-4, 1997.
- 976 Boudries, H., Canagaratna, M. R., Jayne, J. T., Alfarra, M. R., Allan, J., Bower, K. N., Coe, H.,
977 Pryor, S. C., Jimenez, J. L., Brook, J. R., Li, S., and Worsnop, D. R.: Chemical and physical
978 processes controlling the distribution of aerosols in the Lower Fraser Valley, Canada, during
979 the Pacific 2001 field campaign, Atmos. Environm., 38, 5759-5774,
980 10.1016/j.atmosenv.2004.01.057, 2004.
- 981 Brook, J. R., Strawbridge, K. B., Snyder, B. J., Boudries, H., Worsnop, D., Sharma, S., Anlauf,
982 K., Lu, G., and Hayden, K.: Towards an understanding of the fine particle variations in the
983 LFV: integration of chemical, physical and meteorological observations, Atmos. Environm.,
984 38, 5775-5788, 10.1016/j.atmosenv.2004.01.056, 2004.



- 985 Bröske, R., Kleffmann, J., and Wiesen, P.: Heterogeneous conversion of NO₂ on secondary
986 organic aerosol surfaces: A possible source of nitrous acid (HONO) in the atmosphere?, Atmos.
987 Chem. Phys., 3, 469-474, 10.5194/acp-3-469-2003, 2003.
- 988 Brown, S. S., Stark, H., Ciciora, S. J., and Ravishankara, A. R.: In-situ measurement of
989 atmospheric NO₃ and N₂O₅ via cavity ring-down spectroscopy, Geophys. Res. Lett., 28, 3227-
990 3230, 10.1029/2001GL013303, 2001.
- 991 Brown, S. S., Stark, H., Ciciora, S. J., McLaughlin, R. J., and Ravishankara, A. R.:
992 Simultaneous in situ detection of atmospheric NO₃ and N₂O₅ via cavity ring-down
993 spectroscopy, Rev. Sci. Instrum., 73, 3291-3301, 10.1063/1.1499214, 2002.
- 994 Brown, S. S., Stark, H., and Ravishankara, A. R.: Applicability of the steady state
995 approximation to the interpretation of atmospheric observations of NO₃ and N₂O₅, J. Geophys.
996 Res., 108, 4539, doi: 10.1029/2003JD003407, 2003.
- 997 Brown, S. S., Neuman, J. A., Ryerson, T. B., Trainer, M., Dube, W. P., Holloway, J. S.,
998 Warneke, C., de Gouw, J. A., Donnelly, S. G., Atlas, E., Matthew, B., Middlebrook, A. M.,
999 Peltier, R., Weber, R. J., Stohl, A., Meagher, J. F., Fehsenfeld, F. C., and Ravishankara, A. R.:
1000 Nocturnal odd-oxygen budget and its implications for ozone loss in the lower troposphere,
1001 Geophys. Res. Lett., 33, L08801, 10.1029/2006GL025900, 2006a.
- 1002 Brown, S. S., Ryerson, T. B., Wollny, A. G., Brock, C. A., Peltier, R., Sullivan, A. P., Weber,
1003 R. J., Dube, W. P., Trainer, M., Meagher, J. F., Fehsenfeld, F. C., and Ravishankara, A. R.:
1004 Variability in nocturnal nitrogen oxide processing and its role in regional air quality, Science,
1005 311, 67-70, 10.1126/science.1120120 2006b.
- 1006 Brown, S. S., Dube, W. P., Osthoff, H. D., Stutz, J., Ryerson, T. B., Wollny, A. G., Brock, C.
1007 A., Warneke, C., De Gouw, J. A., Atlas, E., Neuman, J. A., Holloway, J. S., Lerner, B. M.,
1008 Williams, E. J., Kuster, W. C., Goldan, P. D., Angevine, W. M., Trainer, M., Fehsenfeld, F. C.,



- 1009 and Ravishankara, A. R.: Vertical profiles in NO₃ and N₂O₅ measured from an aircraft: Results
1010 from the NOAA P-3 and surface platforms during the New England Air Quality Study 2004, J.
1011 Geophys. Res., 112, D22304, 10.1029/2007JD008883, 2007.
- 1012 Brown, S. S., and Stutz, J.: Nighttime radical observations and chemistry, Chem. Soc. Rev., 41,
1013 6405-6447, 10.1039/c2cs35181a, 2012.
- 1014 Brown, S. S., Thornton, J. A., Keene, W. C., Pszenny, A. A. P., Sive, B. C., Dubé, W. P.,
1015 Wagner, N. L., Young, C. J., Riedel, T. P., Roberts, J. M., VandenBoer, T. C., Bahreini, R.,
1016 Öztürk, F., Middlebrook, A. M., Kim, S., Hübler, G., and Wolfe, D. E.: Nitrogen, Aerosol
1017 Composition, and Halogens on a Tall Tower (NACHTT): Overview of a wintertime air
1018 chemistry field study in the front range urban corridor of Colorado, J. Geophys. Res., 118, 8067-
1019 8085, 10.1002/jgrd.50537, 2013.
- 1020 Brown, S. S., Dubé, W. P., Tham, Y. J., Zha, Q., Xue, L., Poon, S., Wang, Z., Blake, D. R.,
1021 Tsui, W., Parrish, D. D., and Wang, T.: Nighttime chemistry at a high altitude site above Hong
1022 Kong, J. Geophys. Res.-Atmos., 121, 2457-2475, 10.1002/2015jd024566, 2016.
- 1023 Chang, W. L., Bhawe, P. V., Brown, S. S., Riemer, N., Stutz, J., and Dabdub, D.: Heterogeneous
1024 Atmospheric Chemistry, Ambient Measurements, and Model Calculations of N₂O₅: A Review,
1025 Aerosol Sci. Technol., 45, 655 - 685, 10.1080/02786826.2010.551672, 2011.
- 1026 Crowley, J. N., Schuster, G., Pouvesle, N., Parchatka, U., Fischer, H., Bonn, B., Bingemer, H.,
1027 and Lelieveld, J.: Nocturnal nitrogen oxides at a rural mountain-site in south-western Germany,
1028 Atmos. Chem. Phys., 10, 2795-2812, 10.5194/acp-10-2795-2010, 2010.
- 1029 Curren, K. C., Dann, T. F., and Wang, D. K.: Ambient air 1,3-butadiene concentrations in
1030 Canada (1995–2003): seasonal, day of week variations, trends, and source influences, Atmos.
1031 Environm., 40, 170-181, 10.1016/j.atmosenv.2005.09.025, 2006.



- 1032 Davidovits, P., Kolb, C. E., Williams, L. R., Jayne, J. T., and Worsnop, D. R.: Mass
1033 accommodation and chemical reactions at gas-liquid interfaces, *Chem. Rev.*, 106, 1323-1354,
1034 2006.
- 1035 HYSPLIT (HYbrid Single-Particle Lagrangian Integrated Trajectory) Model access via NOAA
1036 ARL READY Website <http://ready.arl.noaa.gov/HYSPLIT.php>, 2013.
- 1037 Drewitt, G. B., Curren, K., Steyn, D. G., Gillespie, T. J., and Niki, H.: Measurement of biogenic
1038 hydrocarbon emissions from vegetation in the Lower Fraser Valley, British Columbia, *Atmos.*
1039 *Environm.*, 32, 3457-3466, 10.1016/S1352-2310(98)00043-0, 1998.
- 1040 Dubé, W. P., Brown, S. S., Osthoff, H. D., Nunley, M. R., Ciciora, S. J., Paris, M. W.,
1041 McLaughlin, R. J., and Ravishankara, A. R.: Aircraft instrument for simultaneous, in situ
1042 measurement of NO₃ and N₂O₅ via pulsed cavity ring-down spectroscopy, *Rev. Sci. Instrum.*,
1043 77, 034101, 10.1063/1.2176058, 2006.
- 1044 Edwards, P. M., Brown, S. S., Roberts, J. M., Ahmadov, R., Banta, R. M., deGouw, J. A., Dube,
1045 W. P., Field, R. A., Flynn, J. H., Gilman, J. B., Graus, M., Helmig, D., Koss, A., Langford, A.
1046 O., Lefer, B. L., Lerner, B. M., Li, R., Li, S.-M., McKeen, S. A., Murphy, S. M., Parrish, D. D.,
1047 Senff, C. J., Soltis, J., Stutz, J., Sweeney, C., Thompson, C. R., Trainer, M. K., Tsai, C., Veres,
1048 P. R., Washenfelder, R. A., Warneke, C., Wild, R. J., Young, C. J., Yuan, B., and Zamora, R.:
1049 High winter ozone pollution from carbonyl photolysis in an oil and gas basin, *Nature*, 514, 351-
1050 354, 10.1038/nature13767, 2014.
- 1051 Faxon, C., Bean, J., and Ruiz, L.: Inland Concentrations of Cl₂ and ClNO₂ in Southeast Texas
1052 Suggest Chlorine Chemistry Significantly Contributes to Atmospheric Reactivity, *Atmosphere*,
1053 6, 1487, 10.3390/atmos6101487, 2015.



- 1054 Finlayson-Pitts, B. J., Ezell, M. J., and Pitts, J. N.: Formation Of Chemically Active Chlorine
1055 Compounds By Reactions Of Atmospheric NaCl Particles With Gaseous N₂O₅ And ClONO₂,
1056 Nature, 337, 241-244, 10.1038/337241a0 1989.
- 1057 Geyer, A., and Stutz, J.: Vertical profiles of NO₃, N₂O₅, O₃, and NO_x in the nocturnal boundary
1058 layer: 2. Model studies on the altitude dependence of composition and chemistry, J. Geophys.
1059 Res., 109, D12307, doi:12310.11029/12003JD004211, 2004.
- 1060 Ghosh, B., Papanastasiou, D. K., Talukdar, R. K., Roberts, J. M., and Burkholder, J. B.: Nitryl
1061 Chloride (ClNO₂): UV/Vis Absorption Spectrum between 210 and 296 K and O(³P) Quantum
1062 Yield at 193 and 248 nm, J. Phys. Chem. A, 116, 5796-5805, 10.1021/jp207389y, 2012.
- 1063 Guenther, A., Hewitt, C. N., Erickson, D., Fall, R., Geron, C., Graedel, T., Harley, P., Klinger,
1064 L., Lerdau, M., McKay, W. A., Pierce, T., Scholes, B., Steinbrecher, R., Tallamraju, R., Taylor,
1065 J., and Zimmerman, P.: A Global-Model Of Natural Volatile Organic-Compound Emissions, J.
1066 Geophys. Res., 100, 8873-8892, 10.1029/94JD02950, 1995.
- 1067 Guenther, A. B., Jiang, X., Heald, C. L., Sakulyanontvittaya, T., Duhl, T., Emmons, L. K., and
1068 Wang, X.: The Model of Emissions of Gases and Aerosols from Nature version 2.1
1069 (MEGAN2.1): an extended and updated framework for modeling biogenic emissions, Geosci.
1070 Model Dev., 5, 1471-1492, 10.5194/gmd-5-1471-2012, 2012.
- 1071 Gurren, K., Gillespie, T., Steyn, D., Dann, T., and Wang, D.: Biogenic isoprene in the Lower
1072 Fraser Valley, British Columbia, J. Geophys. Res.-Atmos., 103, 25467-25477,
1073 10.1029/98jd01214, 1998.
- 1074 Hannemann, A. U., Mitra, S. K., and Pruppacher, H. R.: On the scavenging of gaseous nitrogen
1075 compounds by large and small rain drops 1. A wind tunnel and theoretical study of the uptake
1076 and desorption of NH₃ in the presence of CO₂, J. Atmos. Chem., 21, 293-307,
1077 10.1007/bf00696760, 1995.



- 1078 Hayden, K. L., Anlauf, K. G., Hoff, R. M., Strapp, J. W., Bottenheim, J. W., Wiebe, H. A.,
1079 Froude, F. A., Martin, J. B., Steyn, D. G., and McKendry, I. G.: The vertical chemical and
1080 meteorological structure of the boundary layer in the Lower Fraser Valley during Pacific '93,
1081 Atmos. Environm., 31, 2089-2105, 10.1016/S1352-2310(96)00300-7, 1997.
- 1082 Hayden, K. L., Anlauf, K. G., Li, S. M., Macdonald, A. M., Bottenheim, J. W., Brook, J. R.,
1083 and Wiebe, H. A.: Characterization of gaseous nitrogen oxides in the Lower Fraser Valley
1084 during Pacific 2001, Atmos. Environm., 38, 5811-5823, 10.1016/j.atmosenv.2003.12.048,
1085 2004.
- 1086 Heintz, F., Platt, U., Flentje, H., and Dubois, R.: Long-term observation of nitrate radicals at
1087 the Tor station, Kap Arkona (Rugen), J. Geophys. Res., 101, 22891-22910,
1088 10.1029/96JD01549, 1996.
- 1089 Hewitt, C. N., Ashworth, K., Boynard, A., Guenther, A., Langford, B., MacKenzie, A. R.,
1090 Misztal, P. K., Nemitz, E., Owen, S. M., Possell, M., Pugh, T. A. M., Ryan, A. C., and Wild,
1091 O.: Ground-level ozone influenced by circadian control of isoprene emissions, Nat. Geosci., 4,
1092 671-674, 10.1038/ngeo1271, 2011.
- 1093 Hofzumahaus, A., Kraus, A., and Muller, M.: Solar actinic flux spectroradiometry: a technique
1094 for measuring photolysis frequencies in the atmosphere, Appl. Optics, 38, 4443-4460,
1095 10.1364/AO.38.004443, 1999.
- 1096 Indarto, A.: Heterogeneous reactions of HONO formation from NO₂ and HNO₃: a review, Res.
1097 Chem. Intermed., 38, 1029-1041, 10.1007/s11164-011-0439-z, 2012.
- 1098 Jimenez, J. L., Canagaratna, M. R., Donahue, N. M., Prevot, A. S. H., Zhang, Q., Kroll, J. H.,
1099 DeCarlo, P. F., Allan, J. D., Coe, H., Ng, N. L., Aiken, A. C., Docherty, K. S., Ulbrich, I. M.,
1100 Grieshop, A. P., Robinson, A. L., Duplissy, J., Smith, J. D., Wilson, K. R., Lanz, V. A., Hueglin,
1101 C., Sun, Y. L., Tian, J., Laaksonen, A., Raatikainen, T., Rautiainen, J., Vaattovaara, P., Ehn,



- 1102 M., Kulmala, M., Tomlinson, J. M., Collins, D. R., Cubison, M. J., E., Dunlea, J., Huffman, J.
1103 A., Onasch, T. B., Alfarra, M. R., Williams, P. I., Bower, K., Kondo, Y., Schneider, J.,
1104 Drewnick, F., Borrmann, S., Weimer, S., Demerjian, K., Salcedo, D., Cottrell, L., Griffin, R.,
1105 Takami, A., Miyoshi, T., Hatakeyama, S., Shimono, A., Sun, J. Y., Zhang, Y. M., Dzepina, K.,
1106 Kimmel, J. R., Sueper, D., Jayne, J. T., Herndon, S. C., Trimborn, A. M., Williams, L. R.,
1107 Wood, E. C., Middlebrook, A. M., Kolb, C. E., Baltensperger, U., and Worsnop, D. R.:
1108 Evolution of Organic Aerosols in the Atmosphere, *Science*, 326, 1525-1529,
1109 10.1126/science.1180353, 2009.
- 1110 Kercher, J. P., Riedel, T. P., and Thornton, J. A.: Chlorine activation by N₂O₅: simultaneous, in
1111 situ detection of ClNO₂ and N₂O₅ by chemical ionization mass spectrometry, *Atmospheric*
1112 *Measurement Techniques*, 2, 193-204, 10.5194/amt-2-193-2009, 2009.
- 1113 Kim, M. J., Farmer, D. K., and Bertram, T. H.: A controlling role for the air-sea interface in the
1114 chemical processing of reactive nitrogen in the coastal marine boundary layer, *Proc. Natl. Acad.*
1115 *Sci. U.S.A.*, 111, 3943-3948, 10.1073/pnas.1318694111, 2014.
- 1116 Kleinman, L., Lee, Y.-N., Springston, S. R., Nunnermacker, L., Zhou, X., Brown, R., Hallock,
1117 K., Klotz, P., Leahy, D., Lee, J. H., and Newman, L.: Ozone formation at a rural site in the
1118 southeastern United States, *J. Geophys. Res.-Atmos.*, 99, 3469-3482, 10.1029/93jd02991,
1119 1994.
- 1120 Knipping, E. M., and Dabdub, D.: Impact of chlorine emissions from sea-salt aerosol on coastal
1121 urban ozone, *Environm. Sci. Technol.*, 37, 275-284, 10.1021/es025793z 2003.
- 1122 Koehler, G., and Wassenaar, L. I.: The stable isotopic composition (³⁷Cl/³⁵Cl) of dissolved
1123 chloride in rainwater, *Applied Geochemistry*, 25, 91-96, 10.1016/j.apgeochem.2009.10.004,
1124 2010.



- 1125 Lin, C. H., Lai, C. H., Wu, Y. L., and Chen, M. J.: Simple model for estimating dry deposition
1126 velocity of ozone and its destruction in a polluted nocturnal boundary layer, *Atmos. Environm.*,
1127 44, 4364-4371, 10.1016/j.atmosenv.2010.07.053, 2010.
- 1128 Logan, J. A.: Ozone in rural areas of the United States, *J. Geophys. Res.-Atmos.*, 94, 8511-
1129 8532, 10.1029/JD094iD06p08511, 1989.
- 1130 Madronich, S., and Flocke, S.: Theoretical Estimation of Biologically Effective UV Radiation
1131 at the Earth's Surface, in: *Solar Ultraviolet Radiation*, edited by: Zerefos, C., and Bais, A.,
1132 NATO ASI Series, Springer Berlin Heidelberg, 23-48, 1997.
- 1133 McKendry, I. G., Steyn, D. G., Lundgren, J., Hoff, R. M., Strapp, W., Anlauf, K., Froude, F.,
1134 Martin, J. B., Banta, R. M., and Olivier, L. D.: Elevated ozone layers and vertical down-mixing
1135 over the Lower Fraser Valley, BC, *Atmos. Environm.*, 31, 2135-2146, 10.1016/S1352-
1136 2310(96)00127-6, 1997.
- 1137 McLaren, R., Salmon, R. A., Liggio, J., Hayden, K. L., Anlauf, K. G., and Leaitch, W. R.:
1138 Nighttime chemistry at a rural site in the Lower Fraser Valley, *Atmos. Environm.*, 38, 5837-
1139 5848, 10.1016/j.atmosenv.2004.03.074, 2004.
- 1140 McLaren, R., Wojtal, P., Majonis, D., McCourt, J., Halla, J. D., and Brook, J.: NO₃ radical
1141 measurements in a polluted marine environment: links to ozone formation, *Atmos. Chem.*
1142 *Phys.*, 10, 4187-4206, 10.5194/acp-10-4187-2010, 2010.
- 1143 Mielke, L. H., Furgeson, A., and Osthoff, H. D.: Observation of ClNO₂ in a mid-continental
1144 urban environment, *Environm. Sci. Technol.*, 45, 8889-8896, 10.1021/es201955u, 2011.
- 1145 Mielke, L. H., and Osthoff, H. D.: On quantitative measurements of peroxy-carboxylic nitric
1146 anhydride mixing ratios by thermal dissociation chemical ionization mass spectrometry, *Int. J.*
1147 *Mass Spectrom.*, 310, 1-9, 10.1016/j.ijms.2011.10.005, 2012.



- 1148 Mielke, L. H., Stutz, J., Tsai, C., Hurlock, S. C., Roberts, J. M., Veres, P. R., Froyd, K. D.,
1149 Hayes, P. L., Cubison, M. J., Jimenez, J. L., Washenfelder, R. A., Young, C. J., Gilman, J. B.,
1150 de Gouw, J. A., Flynn, J. H., Grossberg, N., Lefer, B. L., Liu, J., Weber, R. J., and Osthoff, H.
1151 D.: Heterogeneous formation of nitryl chloride and its role as a nocturnal NO_x reservoir species
1152 during CalNex-LA 2010, *J. Geophys. Res.*, 118, 10638-10652, 10.1002/jgrd.50783, 2013.
- 1153 Mielke, L. H., Furgeson, A., Odame-Ankrah, C. A., and Osthoff, H. D.: Ubiquity of ClNO₂ in
1154 the nocturnal boundary layer of Calgary, AB, Canada, *Canadian Journal of Chemistry*, 94, 414-
1155 423, 10.1139/cjc-2015-0426, 2016.
- 1156 Neu, U., Kunzle, T., and Wanner, H.: On the relation between ozone storage in the residual
1157 layer and daily variation in near-surface ozone concentration — A case study, *Bound.-Layer*
1158 *Meteor.*, 69, 221-247, 10.1007/bf00708857, 1994.
- 1159 Ng, N. L., Herndon, S. C., Trimborn, A., Canagaratna, M. R., Croteau, P. L., Onasch, T. B.,
1160 Sueper, D., Worsnop, D. R., Zhang, Q., Sun, Y. L., and Jayne, J. T.: An Aerosol Chemical
1161 Speciation Monitor (ACSM) for Routine Monitoring of the Composition and Mass
1162 Concentrations of Ambient Aerosol, *Aerosol Sci. Technol.*, 45, 780-794,
1163 10.1080/02786826.2011.560211, 2011.
- 1164 Odame-Ankrah, C. A., and Osthoff, H. D.: A compact diode laser cavity ring-down
1165 spectrometer for atmospheric measurements of NO₃ and N₂O₅ with automated zeroing and
1166 calibration, *Appl. Spectrosc.*, 65, 1260-1268, 10.1366/11-06384, 2011.
- 1167 Odame-Ankrah, C. A.: Improved detection instrument for nitrogen oxide species, Ph.D.,
1168 Chemistry, University of Calgary, <http://hdl.handle.net/11023/2006>, Calgary, 2015.
- 1169 Osthoff, H. D., Sommariva, R., Baynard, T., Pettersson, A., Williams, E. J., Lerner, B. M.,
1170 Roberts, J. M., Stark, H., Goldan, P. D., Kuster, W. C., Bates, T. S., Coffman, D., Ravishankara,
1171 A. R., and Brown, S. S.: Observation of daytime N₂O₅ in the marine boundary layer during



- 1172 New England Air Quality Study - Intercontinental Transport and Chemical Transformation
1173 2004, *J. Geophys. Res.*, 111, D23S14, doi:10.1029/2006JD007593., 2006.
- 1174 Osthoff, H. D., Pilling, M. J., Ravishankara, A. R., and Brown, S. S.: Temperature dependence
1175 of the NO₃ absorption cross-section above 298 K and determination of the equilibrium constant
1176 for NO₃+NO₂ <-> N₂O₅ at atmospherically relevant conditions, *Phys. Chem. Chem. Phys.*, 9,
1177 5785-5793, 10.1039/b709193a, 2007.
- 1178 Osthoff, H. D., Roberts, J. M., Ravishankara, A. R., Williams, E. J., Lerner, B. M., Sommariva,
1179 R., Bates, T. S., Coffman, D., Quinn, P. K., Stark, H., Burkholder, J. B., Talukdar, R. K.,
1180 Meagher, J., Fehsenfeld, F. C., and Brown, S. S.: High levels of nitryl chloride in the polluted
1181 subtropical marine boundary layer, *Nat. Geosci.*, 1, 324-328, 10.1038/ngeo177, 2008.
- 1182 Paul, D., Furgeson, A., and Osthoff, H. D.: Measurement of total alkyl and peroxy nitrates by
1183 thermal decomposition cavity ring-down spectroscopy, *Rev. Sci. Instrum.*, 80, 114101,
1184 10.1063/1.3258204 2009.
- 1185 Paul, D., and Osthoff, H. D.: Absolute Measurements of Total Peroxy Nitrate Mixing Ratios by
1186 Thermal Dissociation Blue Diode Laser Cavity Ring-Down Spectroscopy, *Anal. Chem.*, 82,
1187 6695-6703, 10.1021/ac101441z, 2010.
- 1188 Phillips, G. J., Tang, M. J., Thieser, J., Brickwedde, B., Schuster, G., Bohn, B., Lelieveld, J.,
1189 and Crowley, J. N.: Significant concentrations of nitryl chloride observed in rural continental
1190 Europe associated with the influence of sea salt chloride and anthropogenic emissions,
1191 *Geophys. Res. Lett.*, 39, L10811, 10.1029/2012gl051912, 2012.
- 1192 Phillips, G. J., Thieser, J., Tang, M. J., Sobanski, N., Schuster, G., Fachinger, J., Drewnick, F.,
1193 Borrmann, S., Bingemer, H., Lelieveld, J., and Crowley, J. N.: Estimating N₂O₅ uptake
1194 coefficients using ambient measurements of NO₃, N₂O₅, ClNO₂ and particle-phase nitrate,
1195 *Atmos. Chem. Phys.*, 16, 13231-13249, 10.5194/acp-16-13231-2016, 2016.



- 1196 Pisano, J. T., McKendry, I., Steyn, D. G., and Hastie, D. R.: Vertical nitrogen dioxide and ozone
1197 concentrations measured from a tethered balloon in the Lower Fraser Valley, Atmos.
1198 Environm., 31, 2071-2078, 10.1016/S1352-2310(96)00146-X, 1997.
- 1199 Pryor, S. C., Barthelmie, R. J., Hoff, R. M., Sakiyama, S., Simpson, R., and Steyn, D.:
1200 REVEAL: Characterizing fine aerosols in the Fraser Valley, BC, Atmosphere-Ocean, 35, 209-
1201 227, 10.1080/07055900.1997.9649592, 1997.
- 1202 Pryor, S. C., and Barthelmie, R. J.: REVEAL II: Seasonality and spatial variability of particle
1203 and visibility conditions in the Fraser Valley, Sci. Tot. Environm., 257, 95-110, 10.1016/S0048-
1204 9697(00)00490-3, 2000.
- 1205 Pryor, S. C., Barthelmie, R. J., Schoof, J. T., Binkowski, F. S., Delle Monache, L., and Stull,
1206 R.: Modeling the impact of sea-spray on particle concentrations in a coastal city, Sci. Tot.
1207 Environm., 391, 132-142, 10.1016/j.scitotenv.2007.10.059, 2008.
- 1208 Raff, J. D., Njegic, B., Chang, W. L., Gordon, M. S., Dabdub, D., Gerber, R. B., and Finlayson-
1209 Pitts, B. J.: Chlorine activation indoors and outdoors via surface-mediated reactions of nitrogen
1210 oxides with hydrogen chloride, Proc. Natl. Acad. Sci. U.S.A., 106, 13647-13654,
1211 10.1073/pnas.0904195106, 2009.
- 1212 Riedel, T. P., Bertram, T. H., Crisp, T. A., Williams, E. J., Lerner, B. M., Vlasenko, A., Li, S.-
1213 M., Gilman, J. B., de Gouw, J., Bon, D. M., Wagner, N. L., Brown, S. S., and Thornton, J. A.:
1214 Nitryl Chloride and Molecular Chlorine in the Coastal Marine Boundary Layer, Environm. Sci.
1215 Technol., 46, 10463-10470, 10.1021/es204632r, 2012a.
- 1216 Riedel, T. P., Bertram, T. H., Ryder, O. S., Liu, S., Day, D. A., Russell, L. M., Gaston, C. J.,
1217 Prather, K. A., and Thornton, J. A.: Direct N₂O₅ reactivity measurements at a polluted coastal
1218 site, Atmos. Chem. Phys., 12, 2959-2968, 10.5194/acp-12-2959-2012, 2012b.



- 1219 Riedel, T. P., Wagner, N. L., Dubé, W. P., Middlebrook, A. M., Young, C. J., Öztürk, F.,
1220 Bahreini, R., VandenBoer, T. C., Wolfe, D. E., Williams, E. J., Roberts, J. M., Brown, S. S.,
1221 and Thornton, J. A.: Chlorine activation within urban or power plant plumes: Vertically
1222 resolved ClNO₂ and Cl₂ measurements from a tall tower in a polluted continental setting, *J.*
1223 *Geophys. Res.*, 118, 8702-8715, 10.1002/jgrd.50637, 2013.
- 1224 Roberts, J. M., Osthoff, H. D., Brown, S. S., Ravishankara, A. R., Coffman, D., Quinn, P. K.,
1225 and Bates, T. S.: Laboratory Studies of Products of N₂O₅ Uptake on Cl⁻ Containing Substrates,
1226 *Geophys. Res. Lett.*, 36, L20808, 10.1029/2009GL040448, 2009.
- 1227 Ryder, O. S., Ault, A. P., Cahill, J. F., Guasco, T. L., Riedel, T. P., Cuadra-Rodriguez, L. A.,
1228 Gaston, C. J., Fitzgerald, E., Lee, C., Prather, K. A., and Bertram, T. H.: On the Role of Particle
1229 Inorganic Mixing State in the Reactive Uptake of N₂O₅ to Ambient Aerosol Particles,
1230 *Environm. Sci. Technol.*, 48, 1618-1627, 10.1021/es4042622, 2014.
- 1231 Ryder, O. S., Campbell, N. R., Morris, H., Forestieri, S., Ruppel, M. J., Cappa, C., Tivanski,
1232 A., Prather, K., and Bertram, T. H.: Role of Organic Coatings in Regulating N₂O₅ Reactive
1233 Uptake to Sea Spray Aerosol, *J. Phys. Chem. A*, 119, 11683-11692, 10.1021/acs.jpca.5b08892,
1234 2015a.
- 1235 Ryder, O. S., Campbell, N. R., Shalowski, M., Al-Mashat, H., Nathanson, G. M., and Bertram,
1236 T. H.: Role of Organics in Regulating ClNO₂ Production at the Air–Sea Interface, *J. Phys.*
1237 *Chem. A*, 119, 8519-8526, 10.1021/jp5129673, 2015b.
- 1238 Sander, R., and Crutzen, P. J.: Model study indicating halogen activation and ozone destruction
1239 in polluted air masses transported to the sea, *J. Geophys. Res.*, 101, 9121-9138,
1240 10.1029/95JD03793, 1996.
- 1241 Sander, S. P., Abbatt, J. P. D., Barker, J. R., Burkholder, J. B., Friedl, R. R., Golden, D. M.,
1242 Huie, R. E., Kolb, C. E., Kurylo, M. J., Moortgat, G. K., Orkin, V. L., and Wine, P. H.: Chemical



- 1243 Kinetics and Photochemical Data for Use in Atmospheric Studies, Evaluation No. 17, JPL
1244 Publication 10-6, Jet Propulsion Laboratory, Pasadena, CA, 2010.
- 1245 Sarwar, G., Simon, H., Xing, J., and Mathur, R.: Importance of tropospheric ClNO₂ chemistry
1246 across the Northern Hemisphere, *Geophys. Res. Lett.*, 41, 4050-4058, 10.1002/2014gl059962,
1247 2014.
- 1248 Seinfeld, J. H., and Pandis, S. N.: Atmospheric chemistry and physics: from air pollution to
1249 climate change, 2nd ed., Wiley, Hoboken, N.J., 2006.
- 1250 Simpson, W. R.: Continuous wave cavity ring-down spectroscopy applied to in situ detection
1251 of dinitrogen pentoxide (N₂O₅), *Rev. Sci. Instrum.*, 74, 3442-3452, 10.1063/1.1578705, 2003.
- 1252 Slusher, D. L., Huey, L. G., Tanner, D. J., Flocke, F. M., and Roberts, J. M.: A thermal
1253 dissociation-chemical ionization mass spectrometry (TD-CIMS) technique for the simultaneous
1254 measurement of peroxyacyl nitrates and dinitrogen pentoxide, *J. Geophys. Res.*, 109, D19315,
1255 10.1029/2004JD004670, 2004.
- 1256 Steyn, D. G., Bottenheim, J. W., and Thomson, R. B.: Overview of tropospheric ozone in the
1257 Lower Fraser Valley, and the Pacific '93 field study, *Atmos. Environm.*, 31, 2025-2035,
1258 10.1016/S1352-2310(97)00018-6, 1997.
- 1259 Stutz, J., Alicke, B., Ackermann, R., Geyer, A., Wang, S. H., White, A. B., Williams, E. J.,
1260 Spicer, C. W., and Fast, J. D.: Relative humidity dependence of HONO chemistry in urban
1261 areas, *J. Geophys. Res.*, 109, D03307, 10.1029/2003JD004135, 2004a.
- 1262 Stutz, J., Alicke, B., Ackermann, R., Geyer, A., White, A., and Williams, E.: Vertical profiles
1263 of NO₃, N₂O₅, O₃, and NO_x in the nocturnal boundary layer: 1. Observations during the Texas
1264 Air Quality Study 2000, *J. Geophys. Res.*, 109, D12306, doi:10.1029/2003JD004209,
1265 2004b.



- 1266 Talbot, R., Mao, H. T., and Sive, B.: Diurnal characteristics of surface level O₃ and other
1267 important trace gases in New England, *J. Geophys. Res.*, 110, D09307,
1268 doi:09310.01029/02004JD005449, 2005.
- 1269 Tanaka, P. L., Riemer, D. D., Chang, S. H., Yarwood, G., McDonald-Buller, E. C., Apel, E. C.,
1270 Orlando, J. J., Silva, P. J., Jimenez, J. L., Canagaratna, M. R., Neece, J. D., Mullins, C. B., and
1271 Allen, D. T.: Direct evidence for chlorine-enhanced urban ozone formation in Houston, Texas,
1272 *Atmos. Environ.*, 37, 1393-1400, 10.1016/S1352-2310(02)01007-5 2003.
- 1273 Thaler, R. D., Mielke, L. H., and Osthoff, H. D.: Quantification of Nitryl Chloride at Part Per
1274 Trillion Mixing Ratios by Thermal Dissociation Cavity Ring-Down Spectroscopy, *Anal.*
1275 *Chem.*, 83, 2761-2766, 10.1021/ac200055z, 2011.
- 1276 Tham, Y., Yan, C., Xue, L., Zha, Q., Wang, X., and Wang, T.: Presence of high nitryl chloride
1277 in Asian coastal environment and its impact on atmospheric photochemistry, *Chin. Sci. Bull.*,
1278 59, 356-359, 10.1007/s11434-013-0063-y, 2014.
- 1279 Tham, Y. J., Wang, Z., Li, Q., Yun, H., Wang, W., Wang, X., Xue, L., Lu, K., Ma, N., Bohn,
1280 B., Li, X., Kecorius, S., Größ, J., Shao, M., Wiedensohler, A., Zhang, Y., and Wang, T.:
1281 Significant concentrations of nitryl chloride sustained in the morning: investigations of the
1282 causes and impacts on ozone production in a polluted region of northern China, *Atmos. Chem.*
1283 *Phys.*, 16, 14959-14977, 10.5194/acp-16-14959-2016, 2016.
- 1284 Thieser, J., Schuster, G., Schuladen, J., Phillips, G. J., Reiffs, A., Parchatka, U., Pöhler, D.,
1285 Lelieveld, J., and Crowley, J. N.: A two-channel thermal dissociation cavity ring-down
1286 spectrometer for the detection of ambient NO₂, RO₂NO₂ and RONO₂, *Atmos. Meas. Tech.*,
1287 9, 553-576, 10.5194/amt-9-553-2016, 2016.
- 1288 Thornton, J. A., Kercher, J. P., Riedel, T. P., Wagner, N. L., Cozic, J., Holloway, J. S., Dube,
1289 W. P., Wolfe, G. M., Quinn, P. K., Middlebrook, A. M., Alexander, B., and Brown, S. S.: A



- 1290 large atomic chlorine source inferred from mid-continental reactive nitrogen chemistry, *Nature*,
1291 464, 271-274, 10.1038/nature08905, 2010.
- 1292 Tokarek, T. W., Huo, J. A., Odame-Ankrah, C. A., Hammoud, D., Taha, Y. M., and Osthoff,
1293 H. D.: A gas chromatograph for quantification of peroxy-carboxylic nitric anhydrides calibrated
1294 by thermal dissociation cavity ring-down spectroscopy, *Atmos. Meas. Tech.*, 7, 3263-3283,
1295 10.5194/amt-7-3263-2014, 2014.
- 1296 Trainer, M., Williams, E. J., Parrish, D. D., Buhr, M. P., Allwine, E. J., Westberg, H. H.,
1297 Fehsenfeld, F. C., and Liu, S. C.: Models and observations of the impact of natural
1298 hydrocarbons on rural ozone, *Nature*, 329, 705-707, 10.1038/329705a0, 1987.
- 1299 Tsai, C., Wong, C., Hurlock, S., Pikel'naya, O., Mielke, L. H., Osthoff, H. D., Flynn, J. H.,
1300 Haman, C., Lefer, B., Gilman, J., de Gouw, J., and Stutz, J.: Nocturnal loss of NO_x during the
1301 2010 CalNex-LA study in the Los Angeles Basin, *J. Geophys. Res.*, 119, 13004–13025
1302 10.1002/2014jd022171, 2014.
- 1303 Vingarzan, R., and Li, S. M.: The Pacific 2001 Air Quality Study - synthesis of findings and
1304 policy implications, *Atmos. Environm.*, 40, 2637-2649, 10.1016/j.atmosenv.2005.09.083,
1305 2006.
- 1306 Volpe, C., Wahlen, M., Pszenny, A. A. P., and Spivack, A. J.: Chlorine isotopic composition
1307 of marine aerosols: Implications for the release of reactive chlorine and HCl cycling rates,
1308 *Geophys. Res. Lett.*, 25, 3831-3834, 10.1029/1998gl900038, 1998.
- 1309 Wagner, N. L., Dube, W. P., Washenfelder, R. A., Young, C. J., Pollack, I. B., Ryerson, T. B.,
1310 and Brown, S. S.: Diode laser-based cavity ring-down instrument for NO₃, N₂O₅, NO, NO₂ and
1311 O₃ from aircraft, *Atmospheric Measurement Techniques*, 4, 1227-1240, 10.5194/amt-4-1227-
1312 2011, 2011.



- 1313 Wang, S., Ackermann, R., and Stutz, J.: Vertical profiles of O₃ and NO_x chemistry in the
1314 polluted nocturnal boundary layer in Phoenix, AZ: I. Field observations by long-path DOAS,
1315 Atmos. Chem. Phys., 6, 2671-2693, 10.5194/acp-6-2671-2006, 2006.
- 1316 Wang, T., Tham, Y. J., Xue, L., Li, Q., Zha, Q., Wang, Z., Poon, S. C. N., Dubé, W. P., Blake,
1317 D. R., Louie, P. K. K., Luk, C. W. Y., Tsui, W., and Brown, S. S.: Observations of nitryl
1318 chloride and modeling its source and effect on ozone in the planetary boundary layer of southern
1319 China, J. Geophys. Res.-Atmos., 121, 2476-2489, 10.1002/2015jd024556, 2016.
- 1320 Wang, X., Wang, H., Xue, L., Wang, T., Wang, L., Gu, R., Wang, W., Tham, Y. J., Wang, Z.,
1321 Yang, L., Chen, J., and Wang, W.: Observations of N₂O₅ and ClNO₂ at a polluted urban surface
1322 site in North China: High N₂O₅ uptake coefficients and low ClNO₂ product yields, Atmos.
1323 Environ., 156, 125-134, 10.1016/j.atmosenv.2017.02.035, 2017.
- 1324 Wayne, R. P., Barnes, I., Biggs, P., Burrows, J. P., Canosamas, C. E., Hjorth, J., Lebras, G.,
1325 Moortgat, G. K., Perner, D., Poulet, G., Restelli, G., and Sidebottom, H.: The Nitrate Radical -
1326 Physics, Chemistry, and the Atmosphere, Atmos. Environ. A, 25, 1-203, 10.1016/0960-
1327 1686(91)90192-A, 1991.
- 1328 Wieser, M. E., and Berglund, M.: Atomic weights of the elements 2007 (IUPAC Technical
1329 Report), Pure Appl. Chem., 81, 2131-2156, 10.1351/pac-rep-09-08-03, 2009.
- 1330 Wild, R. J., Dubé, W. P., Aikin, K. C., Eilerman, S. J., Neuman, J. A., Peischl, J., Ryerson, T.
1331 B., and Brown, S. S.: On-road measurements of vehicle NO₂/NO_x emission ratios in Denver,
1332 Colorado, USA, Atmos. Environ., 148, 182-189, 10.1016/j.atmosenv.2016.10.039, 2017.
- 1333 Wood, E. C., Bertram, T. H., Wooldridge, P. J., and Cohen, R. C.: Measurements of N₂O₅, NO₂,
1334 and O₃ east of the San Francisco Bay, Atmos. Chem. Phys., 5, 483-491, 10.5194/acp-5-483-
1335 2005, 2005.



1336 Young, C. J., Washenfelder, R. A., Roberts, J. M., Mielke, L. H., Osthoff, H. D., Tsai, C.,
 1337 Pikelnaya, O., Stutz, J., Veres, P. R., Cochran, A. K., VandenBoer, T. C., Flynn, J., Grossberg,
 1338 N., Haman, C. L., Lefer, B., Stark, H., Graus, M., de Gouw, J., Gilman, J. B., Kuster, W. C.,
 1339 and Brown, S. S.: Vertically Resolved Measurements of Nighttime Radical Reservoirs in Los
 1340 Angeles and Their Contribution to the Urban Radical Budget, Environm. Sci. Technol., 46,
 1341 10965-10973, 10.1021/es302206a, 2012.

1342 Young, C. J., Washenfelder, R. A., Edwards, P. M., Parrish, D. D., Gilman, J. B., Kuster, W.
 1343 C., Mielke, L. H., Osthoff, H. D., Tsai, C., Pikelnaya, O., Stutz, J., Veres, P. R., Roberts, J. M.,
 1344 Griffith, S., Dusanter, S., Stevens, P. S., Flynn, J., Grossberg, N., Lefer, B., Holloway, J. S.,
 1345 Peischl, J., Ryerson, T. B., Atlas, E. L., Blake, D. R., and Brown, S. S.: Chlorine as a primary
 1346 radical: evaluation of methods to understand its role in initiation of oxidative cycles, Atmos.
 1347 Chem. Phys., 14, 3427-3440, 10.5194/acp-14-3427-2014, 2014.

1348

1349 **Table 1.** Summary of measurement techniques deployed at T45 during the study.

Species or parameter	Method	Uncertainty	Time resolution
CINO ₂ , PAN, PPN	Chemical ionization mass spectrometry (Mielke et al., 2011)	±25% ±10%	30 s
N ₂ O ₅	Red diode laser cavity ring-down spectroscopy (Odame-Ankrah and Osthoff, 2011)	±25%	1 s
O ₃	UV absorption (Thermo 49i)	±10%	10 s
NO/NO _y	O ₃ -Chemiluminescence (Thermo 42i-Y) with heated Mo converter; operated with inlet filter	±30%	10 s
NO ₂	Blue diode laser cavity ring-down spectroscopy (Paul and Osthoff, 2010)	±10%	1 s
PAN, PPN	Gas chromatography with electron capture detection (Tokarek et al., 2014)	±10%	6 min



Photolysis frequencies	Spectral radiometry (Metcon)	±20%	10 s
Aerosol size distribution	Scanning mobility particle sizer (SMPS)		nd
Aerosol composition	Aerosol Chemical Speciation Monitor (ACSM)	±20%	30 min
VOCs	Agilent	±30%	20 min (1 hr [*])
Meteorological data	Various		

1350 * Sampled for 20 min within a 1 hour time period



1351 **Table 2.** Ratios of up- to down-dwelling photolysis frequencies.

Frequency	Ratio
$j(\text{NO}_3)$	0.27 ± 0.04
$j(\text{NO}_2)$	0.15 ± 0.03
$j(\text{ClONO}_2)$	0.14 ± 0.02
$j(\text{O}_3 \rightarrow \text{O}(^1\text{D}))$	0.11 ± 0.02

1352

1353 **Table 3.** Maximum ClNO₂ mixing ratios observed to date.

Location	Type	Maximum mixing ratio	Reference(s)
Houston, TX	Off-shore, costal, and inland	1.2 ppbv	(Osthoff et al., 2008)
New England	Off-shore	90 pptv	(Kercher et al., 2009)
Pasadena, CA	Off-shore	2.15 ppbv	(Riedel et al., 2012a)
La Jolla, CA	Coastal	30 pptv	(Kim et al., 2014)
Boulder, CO	Continental	425 pptv	(Thornton et al., 2010)
Calgary, AB	Continental	330 pptv	(Mielke et al., 2016; Mielke et al., 2011)
Erie, CO	Continental	1.3 ppbv	(Riedel et al., 2013; Brown et al., 2013)
Feldberg, GER	Continental	800 pptv	(Phillips et al., 2012; Phillips et al., 2016)
Horsepool, UT	Continental	500 pptv	(Edwards et al., 2014)
Pasadena, CA	Coastal, inland	3.5 ppbv	(Mielke et al., 2013)
London, UK	Coastal, inland	724 pptv	(Bannan et al., 2015)
Hongkong, PRC	Coastal, inland	2.0 ppbv	(Tham et al., 2014)
Southeast TX	Coastal, inland	280 pptv	(Faxon et al., 2015)
Hongkong, PRC	Coastal, inland	4.7 ppbv	(Wang et al., 2016)
North China Plain	Continental	2.1 ppbv	(Tham et al., 2016)
North China Plain	Continental	776 pptv	(Wang et al., 2017)
Abbotsford, BC	Coastal, inland	97 pptv	This work

1354